UC San Diego
UC San Diego Electronic Theses and Dissertations

Title
Long-Term Dynamics and Special Solutions of Lunar Orbiters

Permalink
https://escholarship.org/uc/item/6zr6x9g8

Author
Patel, Jeet A

Publication Date
2022

Peer reviewed|Thesis/dissertation

UNIVERSITY OF CALIFORNIA SAN DIEGO

Long-Term Dynamics and Special Solutions of Lunar Orbiters

A thesis submitted in partial satisfaction of the
requirements for the degree
Master of Science

in

Engineering Science (Aerospace Engineering)

by

Jeet A. Patel

Committee in charge:

Professor Aaron J. Rosengren, Chair
Professor Robert R. Bitmead
Professor John T. Hwang

2022

The thesis of Jeet A. Patel is approved, and it is acceptable in quality and form

for publication on microfilm and electronically.

University of California San Diego

2022

DEDICATION

This thesis is dedicated to everyone who has used up some of their finite time on this Earth to help me along the way.

EPIGRAPH

Do not go gentle into that good night
Old age should burn and rave at close of day
Rage, rage against the dying of the light.

Dylan Thomas

TABLE OF CONTENTS

LIST OF FIGURES

ACKNOWLEDGEMENTS

VITA

2016 - 2020   Bachelor of Science in Aerospace Engineering, University of Florida

2020 - 2022   Master of Science in Aerospace Engineering, University of California San Diego

ABSTRACT OF THE THESIS

Long-Term Dynamics and Special Solutions of Lunar Orbiters

by

Jeet A. Patel

Master of Science in Engineering Science (Aerospace Engineering)

University of California San Diego, 2022

Professor Aaron J. Rosengren, Chair

New transportation, communication, and logistic infrastructures are being planned and developed for cislunar space in the Earth-Moon system. Cislunar trajectories encompass all of the orbits revolving around the Earth (circumterrestrial) and Moon (circumlunar), as well as those about the Earth-Moon Lagrange point (libration-point orbits) and the various paths between the Earth and Moon (trans-lunar trajectories and transfers). The scope herein is limited to the circumlunar class of orbits, thereby omitting discussions on near-Earth trajectories from low-Earth orbits to the geosynchronous regime, as well as lunar transfers and libration-point orbits. This thesis investigates the long-term dynamics of lunar orbiters, with a particular emphases on special solutions (e.g., frozen and resonant orbits) that have been uncovered in the literature.

NASA's General Mission Analysis Tool (GMAT) is used to provide high-fidelity orbit integrations and dynamical maps, which serve to validate previous analytical and semi-analytical results as well as explore more completely the neighboring phase space.

Introduction

In the 1960's, the Moon came to the forefront of space exploration during the Space Race between the Soviet Union and the United States. The Soviet Union's Luna program, totaling 24 missions, led to the first spacecraft to escape Earth's gravity and the first to orbit another planetary body, among many other astonishing achievements. Almost simultaneously, the U.S. was launching its own missions with the Pioneer program [1]. From 1958 to 1966, most of these missions failed, with some small success involving reaching the Moon via impact, lunar flybys, and returning images from outer space. On 31 March 1966, Luna 10 was launched and a few days later on 3 April 1966, it became the first lunar artificial satellite after orbit insertion [1]. Soon after, Lunar Orbiter I became the first NASA spacecraft to orbit the moon on 14 August 1966. A few years later, with mostly successful missions following from both the Soviet Union and the U.S., Apollo 11 famously landed the first humans on the Moon on 20 July 1969.

After the Apollo and the Luna probes of the early 1970's, there had been a comparative lull in further exploration of the Moon, with the Luna 24 sample return in 1976 representing the last lunar mission for a decade and a half. The first robotic lunar probe since 1976, Japan's Hiten spacecraft, employed a new ballistic capture trajectory, based on weak-stability-boundary theory [2], that used solar perturbations to enable the probe to be temporary captured into circumlunar orbit. This novel low-energy transfer ushered in a new era of space-mission design that was no longer simply predicated on Keplerian motion [3]. The GRAIL Earth-Moon transit was based on this notion of space-manifold dynamics, as was the low-energy trajectories for the two ARTEMIS spacecraft [4].

Whereas modern lunar transfers and libration-point orbits, including the "halo orbit"

planned for the Lunar Gateway and that currently being used by the CNSA's lunar relay satellite [5], Queqiao, are specific applications of the gravitational n-body problem, circumlunar orbits are mainly governed by the perturbed two-body problem, in which the effects of the non-spherical gravity field and third-body perturbations on Moon satellites are often treated in a Hamiltonian formulation (see, e.g.,[6–9]). Given that significant future lunar missions are scheduled or proposed by over a dozen nations or organizations to be launched in this decade, the need for improved understanding of the long-term orbital dynamics about the Moon becomes paramount.

Despite the earliest attempts to characterize the motion of lunar satellites [10–18], which placed emphasis on the construction of analytical, semi-analytical, and numerical theories that were valid in idealized situations or on short mission timescales, our knowledge about the averaged (i.e., long-period and secular) dynamics of circumlunar orbits is still incomplete [19–26]. This Thesis focuses on such long-term dynamics of orbits around the Moon with a particular focus on special solutions to the averaged equations of motions; namely, frozen and Sun-synchronous (resonant) orbits.

Chapter 1

Problem Statement

1.1 Astrodynamics of Lunar Orbiters

The dynamics of a satellite orbiting around Moon is best described by the perturbed two-body problem, which models the deviations from purely Keplerian (two-body) motion. The problem is most readily stated in Cartesian coordinates as $\ddot{\boldsymbol{r}} = -(\mu/r^3)\boldsymbol{r} + \boldsymbol{a}_d$, where $-(\mu/r^3)\boldsymbol{r}$ is the primary (Keplerian) acceleration and $\boldsymbol{a}_d$ is the vector sum of perturbing accelerations due to the gravity of external "third" bodies, non-sphericity of the Moon's gravitational field, solar radiation pressure (SRP), etc. [9, 27]. Rectangular coordinates, which, being in continual rapid change as functions of time, do not clearly disclose the characteristic features of the satellite's motion: accordingly, analytical and semi-analytical formulations consist in regarding the perturbed orbits as ellipses whose elements, shown in Figure 1.1, continually change [28]. The Lagrange planetary equations (LPEs) describing the time-variation of the classical orbital elements under conservative perturbations are given by [28, 29]

$$\frac{\mathrm{d}a}{\mathrm{d}t} = \frac{2}{na}\frac{\partial \mathscr{R}}{\partial M}, \tag{1.1}$$

$$\frac{\mathrm{d}e}{\mathrm{d}t} = \frac{1}{na^2 e}\left((1-e^2)\frac{\partial \mathscr{R}}{\partial M} - \sqrt{1-e^2}\frac{\partial \mathscr{R}}{\partial \omega}\right), \tag{1.2}$$

$$\frac{\mathrm{d}i}{\mathrm{d}t} = \frac{1}{na^2\sqrt{1-e^2}}\left(\cot i\frac{\partial \mathscr{R}}{\partial \omega} - \csc i\frac{\partial \mathscr{R}}{\partial \Omega}\right), \tag{1.3}$$

$$\frac{d\Omega}{dt} = \frac{\csc i}{na^2\sqrt{1-e^2}} \frac{\partial \mathscr{R}}{\partial i},$$ (1.4)

$$\frac{d\omega}{dt} = \frac{\sqrt{1-e^2}}{na^2 e} \frac{\partial \mathscr{R}}{\partial e} - \frac{\cot i}{na^2\sqrt{1-e^2}} \frac{\partial \mathscr{R}}{\partial i},$$ (1.5)

$$\frac{dM}{dt} = n - \frac{2}{na} \frac{\partial \mathscr{R}}{\partial a} - \frac{1-e^2}{na^2 e} \frac{\partial \mathscr{R}}{\partial e},$$ (1.6)

where $\mathscr{R}$ is the disturbing function and is related to the perturbing acceleration by $\boldsymbol{a}_d = \partial \mathscr{R}/\partial t$. Nonsingular formulations of the LPEs exist [30], which are free of the mathematical singularities associated with circular or equatorial orbits that plague the classical equations.

The perturbing forces in astrodynamics can be distinguished as either conservative or non-conservative and as gravitational or non-gravitational. Conservative forces do not change the total energy of the system, on average, whereas non-conservative forces are dissipative [31]. Such forces generally arise from gravitational effects due to the shape and mass distribution of the central body (e.g., planetary oblateness) and the presence of "third" bodies, such as the Earth and Sun in the case of a lunar orbiter. Another minor perturbation considered in this work is that of solar radiation pressure, which, although non-gravitational in nature, can be appropriately modeled as conservative under a reasonably accurate formulation (i.e., adopting the cannonball approximation, which treats the spacecraft as a sphere with constant optical properties, and ignoring the eclipsing of the finite-size solar disk by the solid Moon). Conservative perturbative forces can be characterized by a disturbing function $\mathscr{R}$ and, accordingly, modeled using the LPEs. Non-conservative forces, on the other hand, result from atmospheric drag or discontinuous SRP, and cause energy dissipation. Given that the Moon has a very tenuous atmosphere, causing an otherwise negligible effect on the motion of a lunar orbiter, this work considers only the conservative perturbations arising from the lunar gravity field, the Earth and Sun (treated as distant third body point masses), and continuous solar radiation pressure. It should be noted that SRP causes only minor effects on satellites of low area-to-mass ratio and thus more precisely modeling this non-gravitational perturbation, which requires specific details on the spacecraft's
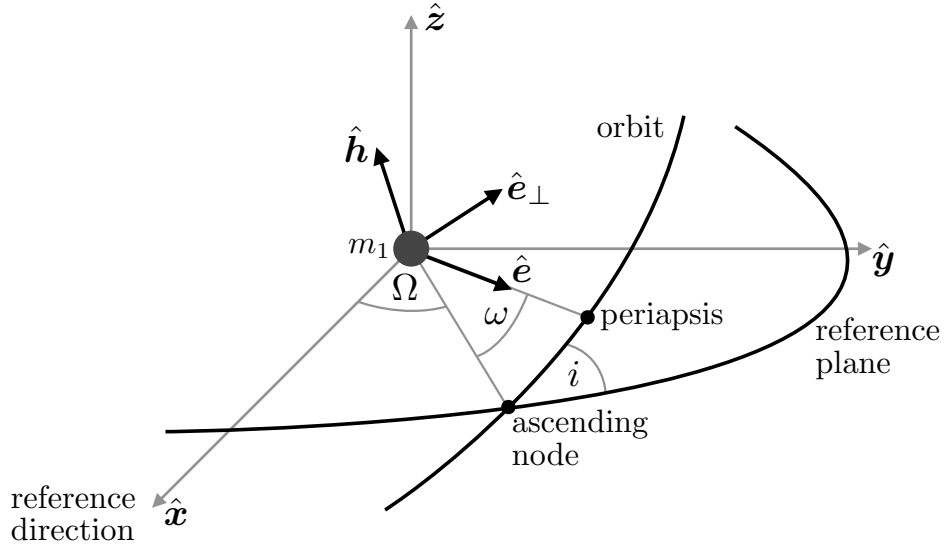
(a) Orientation of the orbital plane in space, described by the three Euler angles: inclination i, longitude of the ascending node Ω, and argument of periapsis ω.
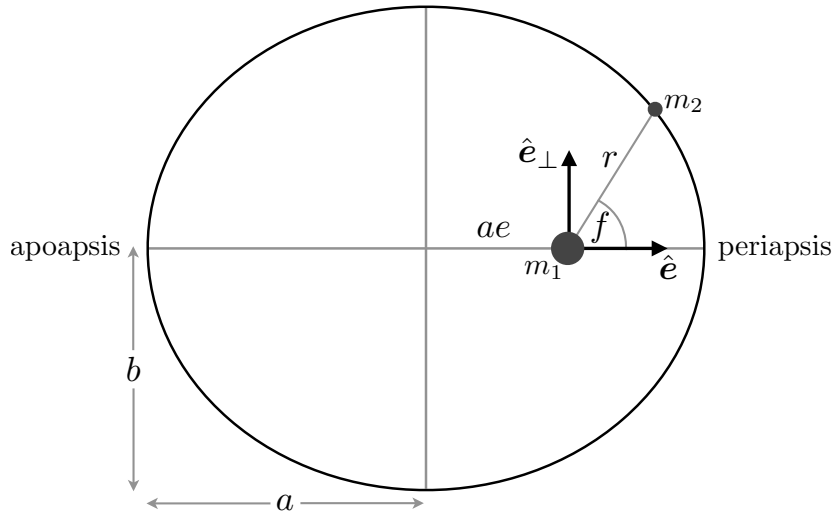
(b) Geometry of the ellipse of eccentricity e, semi-major axis a, and semi-minor axis $b = a\sqrt{1-e^2}$.

Figure 1.1. Geometrical description of the classical orbital elements $(a, e, i, \Omega, \omega, \tau)$. The time since periapsis passage, τ, cannot be displayed, but is linked to the satellite's true anomaly f through Kepler's equation: $M = n(t - \tau) = E - e \sin E$, where E is the eccentric anomaly (see, e.g., [27], for more details). The unit vectors $\hat{\boldsymbol{h}}$ and $\hat{\boldsymbol{e}}$ are the orientation-defining integrals of the two-body problem and can be specified using the Euler angles relative to an inertial frame [29].

optical properties and shape, is out of scope. The discriminating and peculiar features in the problem of a lunar satellite must be taken into account in the study of the averaged orbital dynamics. Thus, while few gravitational harmonics and a simple modeling of the Earth's gravitational field provides sufficiently accurate results for orbits above, say, two planetary radii, disturbances due to mass concentrations below the lunar surface, or mascons, lead to important short-term effects for circular, polar, low-altitude orbiters and an accurate modeling requires the full potential plus the third-body effects [21, 32].

Perturbed Keplerian motion is a multiscale problem [33], in which the (osculating) orbital elements evolve slowly when compared to the change with time t, whose fast evolution is determined by the rate of variation of the mean anomaly M. This bears out the notion of separation of perturbing effects into periodic and secular variations and the distinction between fast and slow time variables. The basic idea in orbit-averaging methods is to obtain approximate equations for the system evolution that contain only slowly changing variables by exploiting the presence of a small dimensionless parameter ε that characterizes the size of the perturbation [6, 7]. The tacit assumption is that the perturbing forces are sufficiently weak so that these approximate averaged equations of motion can be used to describe the secular and long-period orbital evolution [33]. The perturbation equations, relating the time variation of the orbit parameters to the perturbing accelerations, are nonlinear first-order differential equations of the general form

$$\dot{\boldsymbol{\alpha}} = \varepsilon \boldsymbol{g}(\boldsymbol{\alpha}, t), \tag{1.7}$$

where $\boldsymbol{g}(\boldsymbol{\alpha}, t)$ is assumed to be T-periodic in t. Equation 1.7 is trivially solved when $\varepsilon = 0$, yielding the classical elements $\boldsymbol{\alpha} = (a, e, i, \Omega, \omega, \tau)$ in the unperturbed problem. The method of averaging consists in replacing Equation 1.7 by the averaged autonomous system

$$\dot{\bar{\boldsymbol{\alpha}}} = \varepsilon \bar{\boldsymbol{g}}(\bar{\boldsymbol{\alpha}}), \tag{1.8}$$

6

$$\bar{\boldsymbol{g}}(\bar{\boldsymbol{\alpha}}) = \frac{1}{T} \int_0^T \boldsymbol{g}(\boldsymbol{\alpha}, t) \, \mathrm{d}t, \tag{1.9}$$

in which the average is performed over time, and it is understood that $\boldsymbol{\alpha}$ in the integrand is to be regarded as a constant during the averaging process. A characteristic feature of the classical LPEs is that the disturbing function can be averaged prior to application to the system [29]. The averaged disturbing function is defined as

$$\bar{\mathscr{R}}(\boldsymbol{\alpha}) = \frac{1}{2\pi} \int_0^{2\pi} \mathscr{R}(\boldsymbol{\alpha}, M) \, \mathrm{d}M, \tag{1.10}$$

where the averaging is performed over the mean anomaly through the transformation $t = M/n$ (the orbit period $T = 2\pi/n$, where $n = \sqrt{\mu/a^3}$ is the orbital mean motion), while keeping the remaining orbital elements constant.

Due to the Moon's irregular internal structure and complex mass distribution, the effects of the lunar gravitational potential cannot be described with a small number of terms, as in the case for Earth satellites [32]. As a result of the localized gravitational anomalies, the spherical harmonic model, which exhibits a slow convergence as the orbit radius approaches the Moon's surface, requires an overabundance of gravity-field coefficients to properly described them. As an example, for a local anomaly whose angle subtends 1 degree, a 180th order expansion would be required. These local mass concentrations (mascons), shown in Figure 1.2, are defined as "localized regions of higher than average density that produce measurable gravity anomalies [32]." Such anomalies result because mascons have an average density of 3.3 $\frac{g}{cm^3}$ whereas the Moon in general has a density of 3 $\frac{g}{cm^3}$. Mascons, typically found along the equator in lunar seas on the near side of the Moon, constitute only 0.03 percent of the Moon's total mass yet can have a significant long-term impact on low-altitude, lunar orbiters.

Cislunar space in general has some interesting qualities that separate it from the dynamical environments around other celestial bodies [34]. Apart from a free-return trajectory being possible and the Moon being tidal-locked with the Earth due to respective matching of its sidereal

7
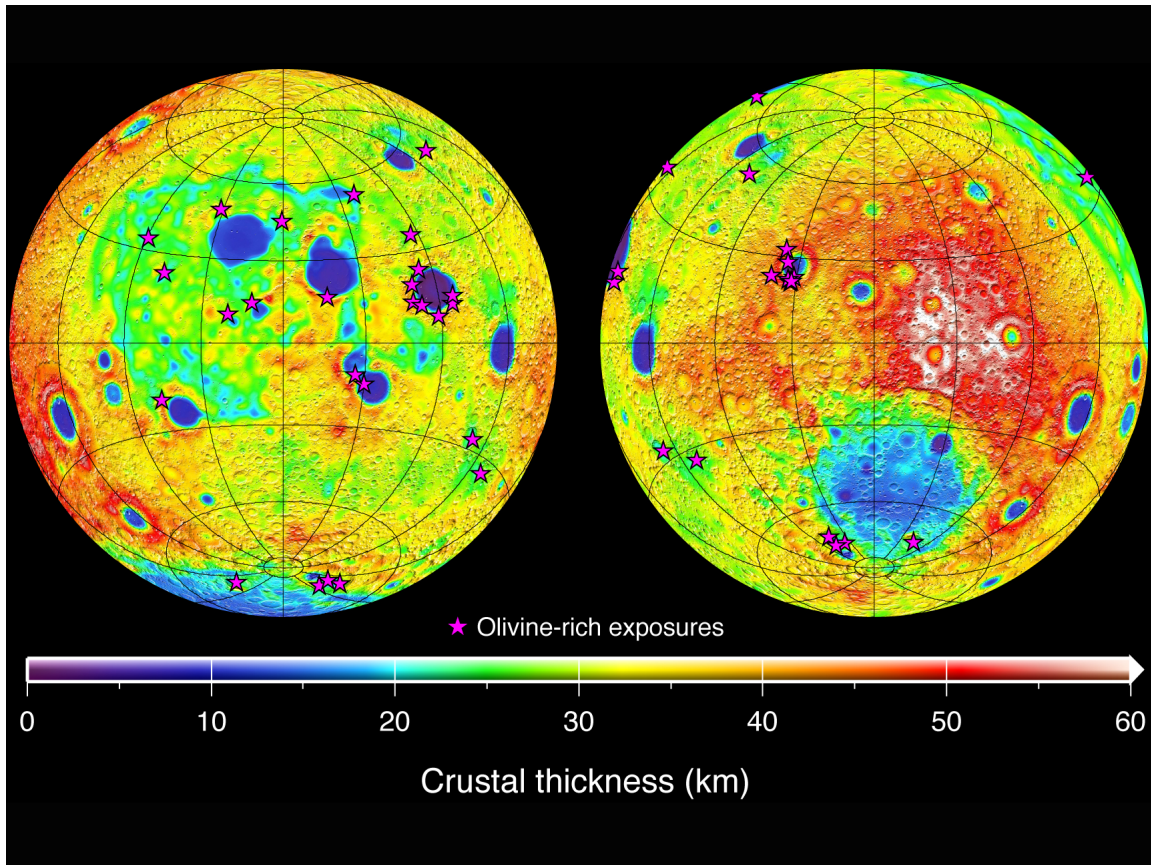
Figure 1.2. This figure illustrates the distribution of mascons across the lunar surface. These high density regions cause gravitational anomalies that must be taken into account, particularly for low-altitude orbits. (Image credit: NASA / JPL-Caltech)

rotational period and orbital mean motion, there are a few other considerations that must be understood in order to analyze lunar orbiters [14, 35]. The lunar orbital plane is inclined relative to the ecliptic plane at $5.9°$ and it regresses around the pole of the ecliptic with a period of 18.6 years. For long-term, Earth-satellite dynamics, a reasonable approximation is to assume that the lunar orbital plane lies in the ecliptic and to subsequently average over its nodal precession [36]. This simplification cannot be made in the case of lunar orbiters, as the Moon's nodal motion causes the fundamental reference direction, used to define the satellite orbit Euler angles, to change [9].

1.2   Special Orbital Solutions for Artificial Lunar Satellites

While seminal work conducted in the Luna and Apollo era centered around uncovering the main perturbing effects on lunar satellite orbiters and on specific mission applications [10, 11, 13–18, 37, 38], current directions are focused on finding long-term stable orbits throughout all of circumlunar space [21, 22, 32, 39, 40]. Frozen orbits correspond to equilibria for the averaged equations of motion, or, as [41] noted, for a dynamical system fabricated to represent the averaged orbital behavior of the satellite. Such secular equilibria, under various dynamical environments, have attracted a lot of attention in Earth-satellite missions [41–43] and planetary satellite and small-body orbiters [9, 44, 45]. In near-Earth space, where the dominant perturbations arise from planetary oblateness, the existence of frozen orbits is attributed to the dynamical balancing of the secular effects of the even zonal harmonics with the long-periodic perturbations of the odd zonal harmonics [42]. These types of orbits with stationary perigee and eccentricity, on average, are of special interest because they minimize altitude variations using only the natural dynamics. Accordingly, they reduce station-keeping requirements and maintain the relative configuration of clusters of satellites [43].

Although the frozen-orbit definition is tied to the averaged equations of motion, these stationary solutions when recast in osculating space can also be identified as periodic orbits in the meridian plane of the satellite, and as quasi-periodic in the three-dimensional space [46]. The direct computation of frozen, periodic orbits can thus be performed directly from the non-averaged equations, and, when accounting for other perturbations, can be done using an optimization routine. Explicit analytical solutions, nevertheless, form the starting point for the numerical optimization process. Lunar frozen orbits, in particular, have been investigated by [1, 9, 23, 47–52]. The Moon's complex gravity field makes finding frozen orbits or quasi-frozen orbits more difficult than in the case for the Earth [32], where only a zonal harmonics model can be used for low-altitude orbits. In contrast to the Earth, where the second degree-and-order gravity field coefficient (C_{22}) is roughly three orders-of-magnitude smaller than the dynamical

oblateness ($J_2 = C_{20}$), these coefficients differ by a factor of about 10 for the Moon [8, 9, 53]. The tesseral harmonics in the lunar potential, coupled with significant Earth third-body perturbations, thus destroy the frozen-orbit conditions of the zonal-only problem.

Given that the Earth's mass is more than 80 times that of the Moon, Earth perturbations on circumlunar orbits are also much more dominant than those caused by the Moon on circum-terrestrial orbits [54]. The Laplace radius is the critical distance at which the Laplace plane lies halfway between the primary body's equatorial and orbital planes [55, 56]: it is thus the distance where the effects of oblateness and third-body forces are equal [14, 36, 57–59]. The Laplace radius for lunar satellites occurs at an altitude of just below 2300 km, whereas for Earth orbiters, the Laplace radius is at a geocentric altitude of nearly 42,700 km (i.e., nearly 7000 km above the geostationary belt). There exist three mutually perpendicular planes of equilibrium for the gravitational motion of bodies under the perturbing action of a distant third-body and from the oblateness of the central body: the classical Laplace plane, characteristic of satellite systems [36], and the remaining two planes discovered by [57] and treated recently in great detail by [55, 59]. [55] defines the Laplace equilibria to be orbits in which the secular evolution due to the quadrupole potential of these gravitational perturbations is zero. Laplace equilibria exist for both circular and eccentric orbits in three planes: the classical, orthogonal, and polar Laplace planes. The orbit poles of the circular Laplace equilibria lie along three orthogonal directions, two of them in the principal plane defined by the central body's rotation pole and orbit pole, and the remaining in the direction orthogonal to this plane. Their stability was investigated by [58] and [59], and subsequently studied independently by [55]. Circular orbits in the classical Laplace plane are generally stable, circular orbits in the orthogonal Laplace plane are always unstable, while those in the polar Laplace plane, which cross over the pole, are stable at small distances where the oblateness perturbation dominates and are unstable otherwise. The Laplace equilibria have not, hitherto, been investigated for lunar satellite orbits and are a central topic of this work.

While there is an abundance of literature exploring lunar frozen orbits and other secular equilibria, there is a comparative lack of comprehensive analysis and results stemming from a full-

scale gravity model. As lunar gravitational harmonics are extremely important for circumlunar orbits at low altitudes, this becomes a major area of interest for future research as parking orbits and lunar hoppers will be an important part of the Artemis accord. Earlier studies have adapted simplified models or poorly estimated gravity-field coefficients; however, with the recent the GRAIL mission, the lunar potential has been mapped more accurately than ever, prompting detailed investigation and validation of special orbital solutions uncovered in earlier analytical, semi-analytical, and numerical analyses.

Chapter 2

Methodology

2.1 Orbital Parameter Space of Previous Lunar Satellite Missions

As a systematic study of the entire parameter space represents a formidable task with significant computational requirements, we first map the orbital distributions in semi-major axis, eccentricity, and inclination of all previous lunar satellite missions. Their orbits in inertial space are shown in Figure 2.1, with their respective ground-tracks, overlaid on a Mercator projection of the lunar surface, given in Figure 2.2. Figures 2.3 and 2.4 show the respective (a, e, i) used by these satellites, which permitted us to narrow the scope of orbital parameter space considered in this study. Orbits of low altitude and eccentricity were used more frequently, but, otherwise, there are no recognizable patterns, as is the case for Earth satellites.

2.2 Analysis of Existing Results

Figure 2.5 seeks to obtain an idea of the differences present between the analytical formulations from literature and the those of numerical integration. As the analytical formulations are done with ideal conditions and simplifications in mind, there will be a noticeable amount of inaccuracy. Figure 2.5 illustrates that although these variations are small initially, they begin to grow substantially at higher altitudes. The analytical formulations were taken with the goal of matching the results from [14] in mind.
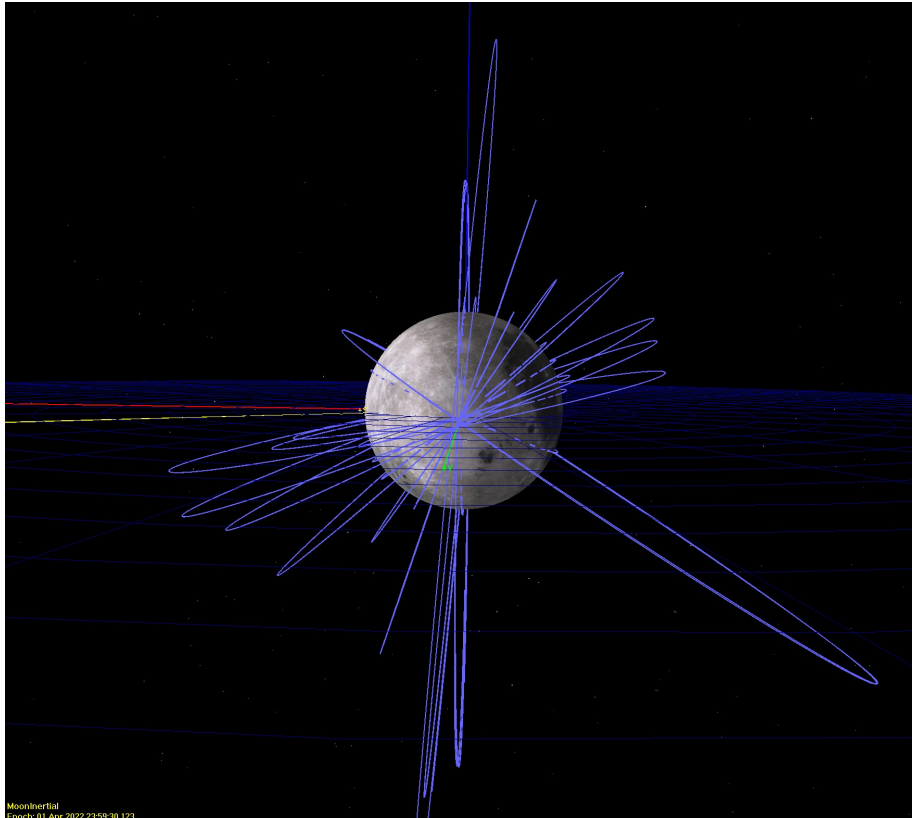
Figure 2.1. The initial orbits of historical lunar satellites, plotted using `GMAT` with data obtained from https://nssdc.gsfc.nasa.gov/. Note that both Ω and ω were artificially set to zero for visualization purposes, thereby showcasing the (a, e, i) distributions.

Figure 2.2. The ground-tracks of historical lunar satellite orbits over one orbital period, plotted using `GMAT` with data obtained from https://nssdc.gsfc.nasa.gov/.

Figure 2.3. A three-dimensional representation of the distribution of semi-major axis, eccentricity, and inclination for all previous lunar satellite mission. Data taken from https://nssdc.gsfc.nasa.gov/.

For the J_2 perturbations, it can be noted that the analytical solution seems to overestimate the rate relative to the numerical solution. Th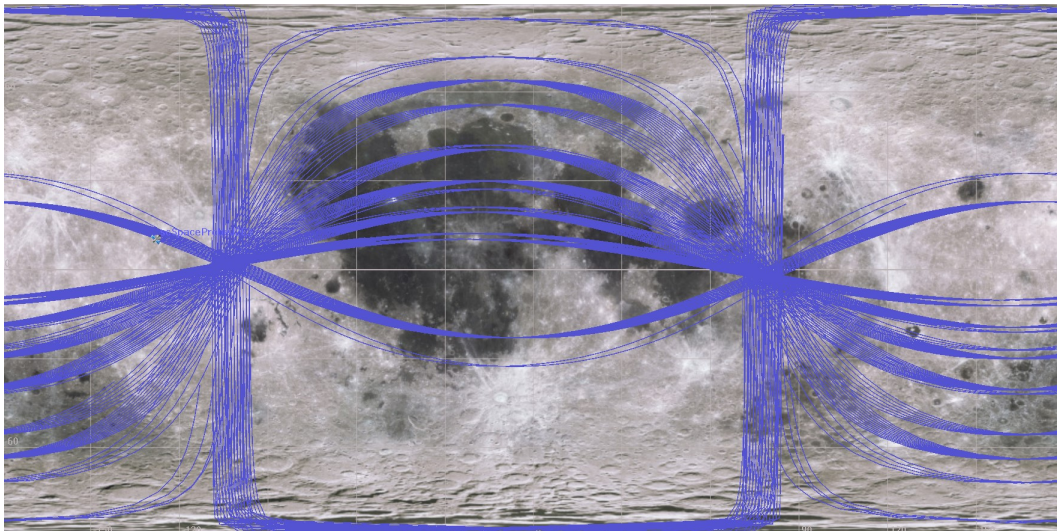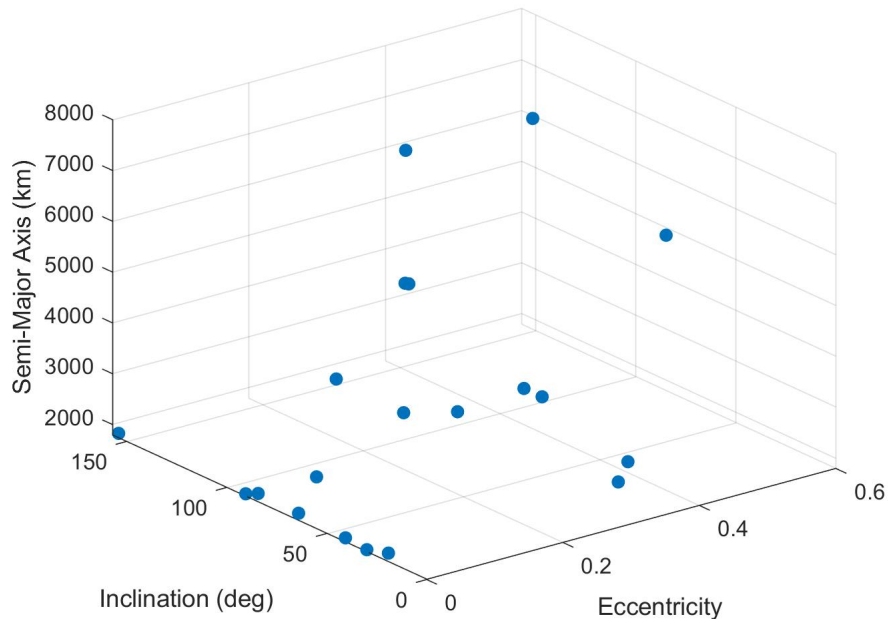e relative error between the analytical and numerical solution for this case seems to be the greatest in regards to the other curves. The relative error between the two seems to grow as the orbital radius increases as well.

For the nodal regression due to 3rd body perturbations due to the Earth, the relative error between the two appears to slowly grow as the semi-major axis increases. The numerical solution also appears to display increasingly oscillatory and diverging behaviour as the orbital radius increases. This is to be expected as the lunar orbiter would begin feeling much more gravitational forces the closer it gets to Earth [27]. The lunar orbiter would also be closer to leaving the Moon's hill sphere, which is much smaller than that of Earth.

For the nodal regression due to the 3rd body perturbations due to the sun, the difference between the analytical and numerical solution appears to be the least out of the three groups. The

14
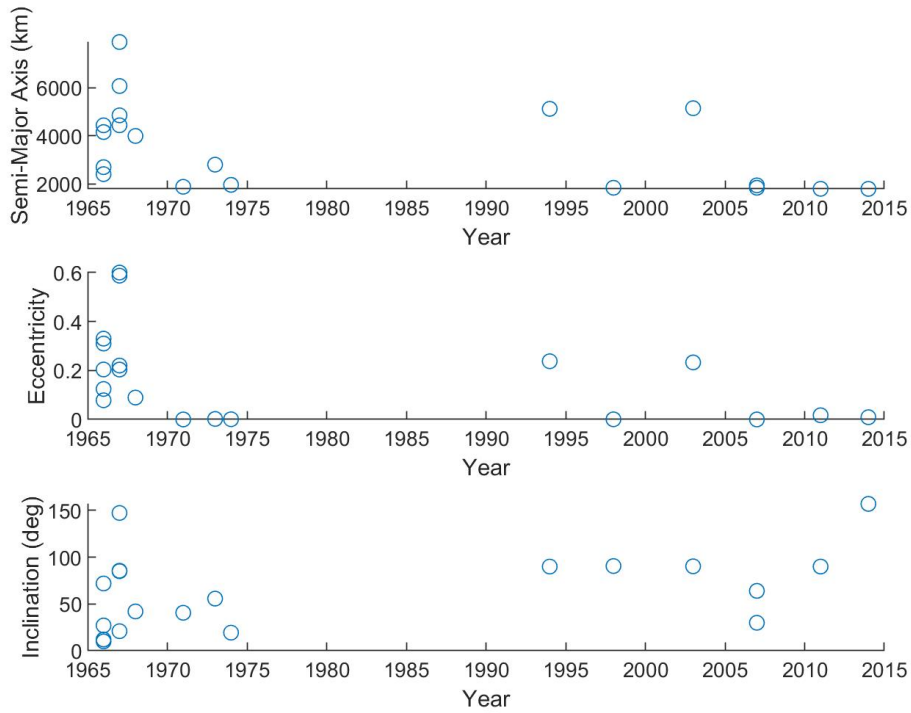
(a) Chronological orbital element distributions of lunar satellite missions.
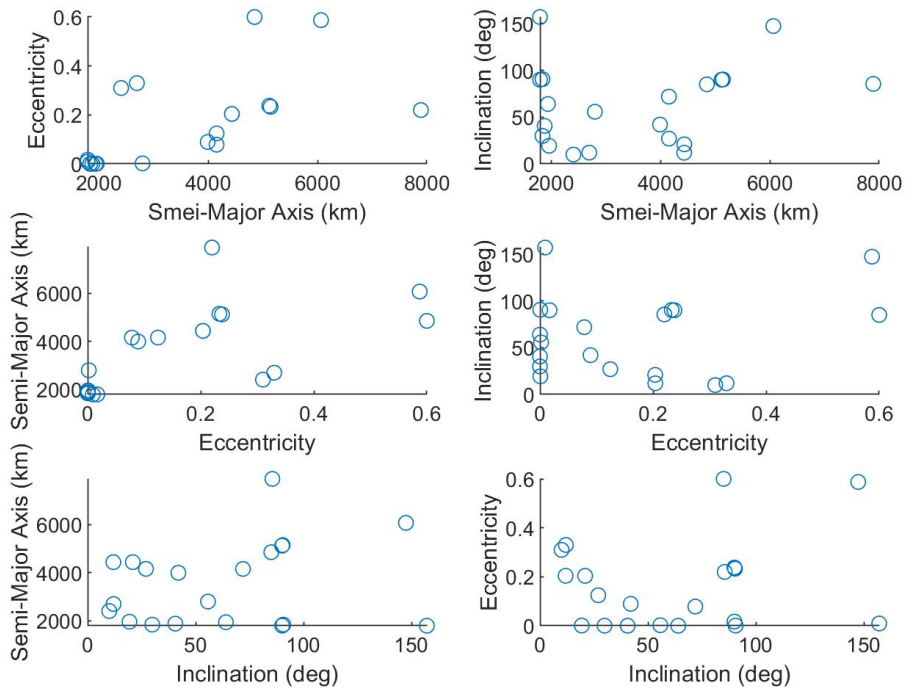
(b) Distribution of (a, e, i) for historical missions.

Figure 2.4. Historic lunar satellite mission orbits in the semi-major axis, eccentricity, and inclination parameter space.

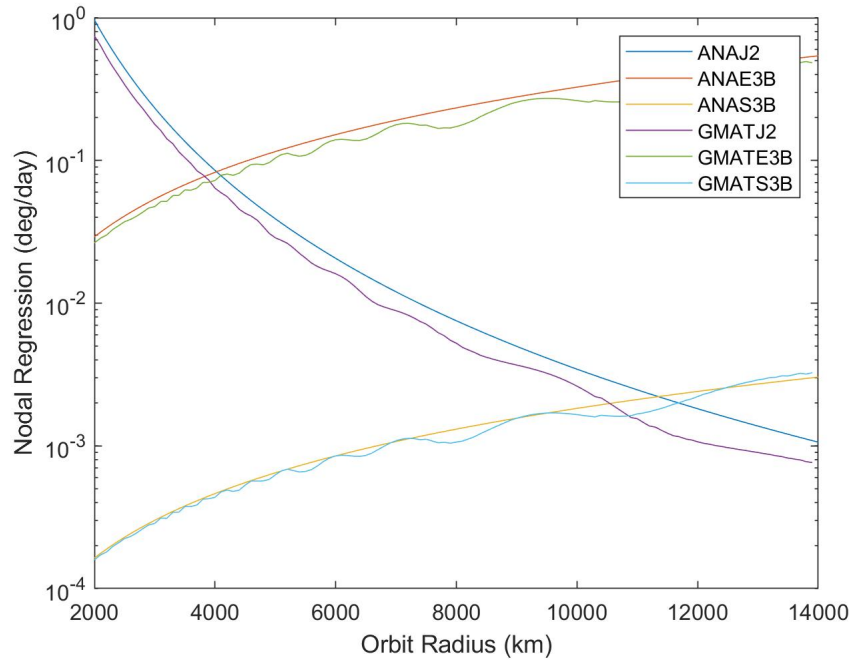**Figure 2.5.** A comparison of the analytical and numerical results for orbit precession. The orbit precession over the course of a day were taken for lunar satellites experiencing the forces mentioned earlier. These results were taken for initial conditions involving a varying semi-major axis of [2000:10:14000]. The eccentricity was set to 0.05 and the inclination to 5 degrees. The Ω and ω were not mentioned in the literature and were set to 0. This figure sought to replicate the results of [14]

magnitude of the perturbations are also much smaller and therefore grow much more slowly as the orbital radius increases. This is to be expected as the ratio of the lunar orbiter's orbital radius to that of the distance from the sun is extremely small and the changes are relatively microscopic. The numerical solution begins to display the same oscillatory behavior as the E3B curves.

As noted earlier, the Moon's oblateness is much less than the Earth's. The rather extreme oblateness difference arises due to the fact that the Earth rotates at the angular velocity of about 360°/day, in contrast to the Moon, which rotates at the relatively stolidly angular rate of about 360°/(27.32 days), giving the Moon a much more spherical shape. Accordingly, the oblateness-induced orbital precession for lunar satellite is comparatively less (see, e.g., Figure 3.3). For circumterrestrial orbits, this perturbation has been depended upon to cause near polar orbits to precess about a degree/day and therefore provide Sun-synchronous orbits that are attractive

for many remote-sensing applications. For the Moon, however, imposing the Sun-synchronous condition is not as attractive for lunar mapping missions as the resulting resonant orbits do not pass sufficiently near the lunar poles. The precession of the line of nodes due to oblateness (J_2 effect only), averaged over an orbital period, is given by the classical result:

$$\dot{\Omega} = -\frac{3}{2}J_2 \left(\frac{R}{p}\right)^2 n\cos i, \quad p = a\left(1 - e^2\right), \quad n = \sqrt{\frac{\mu}{a^3}}. \tag{2.1}$$

A Sun-synchronous orbit requires that

$$\dot{\Omega} = \left(\frac{27.32}{365.25}\right) 360 = 26.9266 \text{ (degrees/lunar day)}.$$

That is, e.g., for a semi-major axis $a = 1837.63$ km, eccentricity $e = 0$, lunar equatorial radius $R = 1737.63$ km, lunar gravitational constant $\mu = 4902.78$ km^3/s^2, lunar second zonal harmonic coefficient $J_2 = 0.00020433$, then the orbit inclination $i = 144.8218°$. Thus, near-polar orbits are not attainable when accounting for Moon oblateness alone. Accordingly, additional perturbations, including SRP, acting in concert will be investigated to produce desirable Moon-sensing mission orbits.

$$\frac{d\Omega}{dt} = -\frac{3}{16}\frac{\mu' \cos(i)(2 - 3\sin^2(i'))}{na'^3(1 - e^2)^{\frac{1}{2}}(1 - e'^2)^{\frac{3}{2}}}(2 + 3e^2) \tag{2.2}$$

The figures below were produced in `GMAT` starting with a set of initial conditions after which the spacecraft was propagated for a period of 100 days. Both simulations used the same epoch and force model. For the force model, only the J_2 effect and 3$^{\text{rd}}$ body perturbations from the Earth were accounted for in the simulation. The initial conditions used were [a, e, i, Ω, ω, v] = [4000, 0.3, 87, 237.35, 69, 63.62] for Figure 2. The semi-major axis and inclination were both chosen from the solutions and literature in order to create a model of an orbit that lacks nodal precession. The other elements were chosen almost arbitrarily. For Figure 3, the

initial conditions used were [a, e, i, Ω, ω, ν] = [8000, 0.3, 40, 237.35, 69, 63.62]. This time, the semi-major axis and inclination were chosen to create an orbit that had a purposeful exaggerated nodal precession.
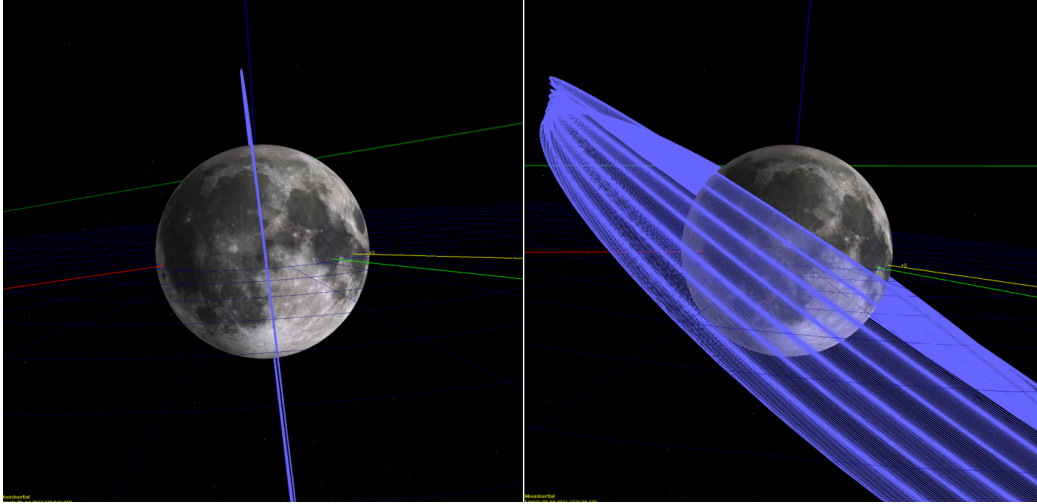
Figure 2.6. (Left) The `GMAT` display for an orbit located in the Laplace plane. In this orbit, the perturbations that would originally shift the RAAN are all near zero. This can be seen as there is no "width" to the orbit, showing that it does not precess. One can note, however, that the semi-major axis and eccentricity still change due to 3rd body effects. (Right) The `GMAT` display for an orbit which experiences a relatively large magnitude of perturbations. The RAAN drift is clearly seen as the orbit appears to have "width" and precesses. There is a change in the semi-major axis and eccentricity as well. This type of orbit would require large amounts of stationkeeping and therefore would not be economic nor realistically sustainable.

Figure 2.7. The same orbits as above were run, with the exception being the settings in the `GMAT` propagator were changed as to increase the truncation and create a higher fidelity model. The degree and order of the calculations for the zonal harmonics were also increased. The frozen orbit displays no change, displaying the robustness of the system. However, the unstable orbit sees relatively massive changes in node precession. This is to be expect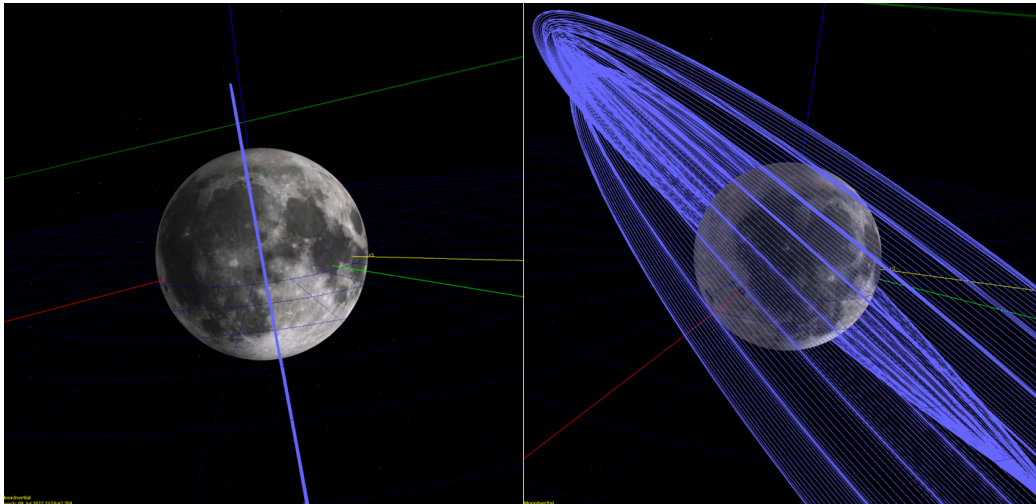ed as there were more zonal harmonics at play and therefore more perturbations if the orbit is not oriented in a stable manner.

2.3   NASA's General Mission Analysis Tool

For the purpose of this thesis in particular, `GMAT` was an invaluable tool for the simulation of lunar orbits through numerical propagation. The software made possible the testing of a multitude of analytical theories along with results from a plethora of papers. The testing of analytical theories allowed for comparison and error estimation between theory and actual numerical simulation. This type of analysis would be useful for the future runs as numerical simulations are time consuming and require an assortment of resources whereas analytical expressions can be calculated with shorter time requirements. The comparison allows one to know which future runs could opt for faster calculations from the theory and which runs would require a more robust numerical simulation. Running orbit simulations also proved valuable as it allowed for the verification of results from previous papers which are used throughout this thesis. The verification of these results gives confidence in the validity of the program being used. This helps

19

in the creation of new results as there is a degree of certainty that the new results will be accurate due to the validation of the results from the literature.

GMAT's propagators offer a high degree of accuracy and fidelity which can be toggled depending on the settings desired by the user. The propagators used in the propagations of this thesis used a 89th order Runge Kutta solver and defined a truncation accuracy to the 10^{-11} degree. The step sizes in the integration could also be defined and were varied depending on the trade-off of accuracy desired and time allowed. The propagators call a set of predefined force models that define the physics of the simulation being run. The plethora of possible settings for these force models were perfectly compatible with the forces present in the orbits that were to be simulated. The force models had options for changing the primary body, selecting any amount of outside point masses to simulate third body effects, allowing for atmospheric drag, and including solar radiation pressure. The force models could also define the degree and order of the gravity field to use for the central body. Due to the multitude of gravitational harmonics at play on the Moon, this was beneficial for selecting the desired truncation on these harmonics. Simulations involving J_2 could be run with just as much ease as a 64x64 simulation of the gravitational field. Albeit one would take exponentially more time to run. The force models also allow the use to define the set of gravity field data being used. For the missions run for this thesis, the LP165P data file was used as it includes much more robust calculations from more recent lunar probes.

GMAT also allows for multiple simulations to be done in each run. Each run can have anywhere from 1 to 1000 spacecraft being propagated. Each of these can start with different initial conditions and can be affected by different sets of force models. The initial conditions cover the range of all the orbital elements and epochs. This allows for the comparison of changes caused by different settings in the orbit regime and was useful for the objectives of this thesis. The inertial frame from which the orbital elements are referenced can also be changed and in general, GMAT allows for the user to select from an array of different orbit coordinate frames. Once the runs are completed, GMAT creates report files which can be easily interpreted by MATLAB and processed for comparison and visualization purposes. The data in the generated report files can be in any

format and can include different kinds of variables that pertain to the simulations run ranging from Keplerian orbital elements, Cartesian elements, and time elapsed.

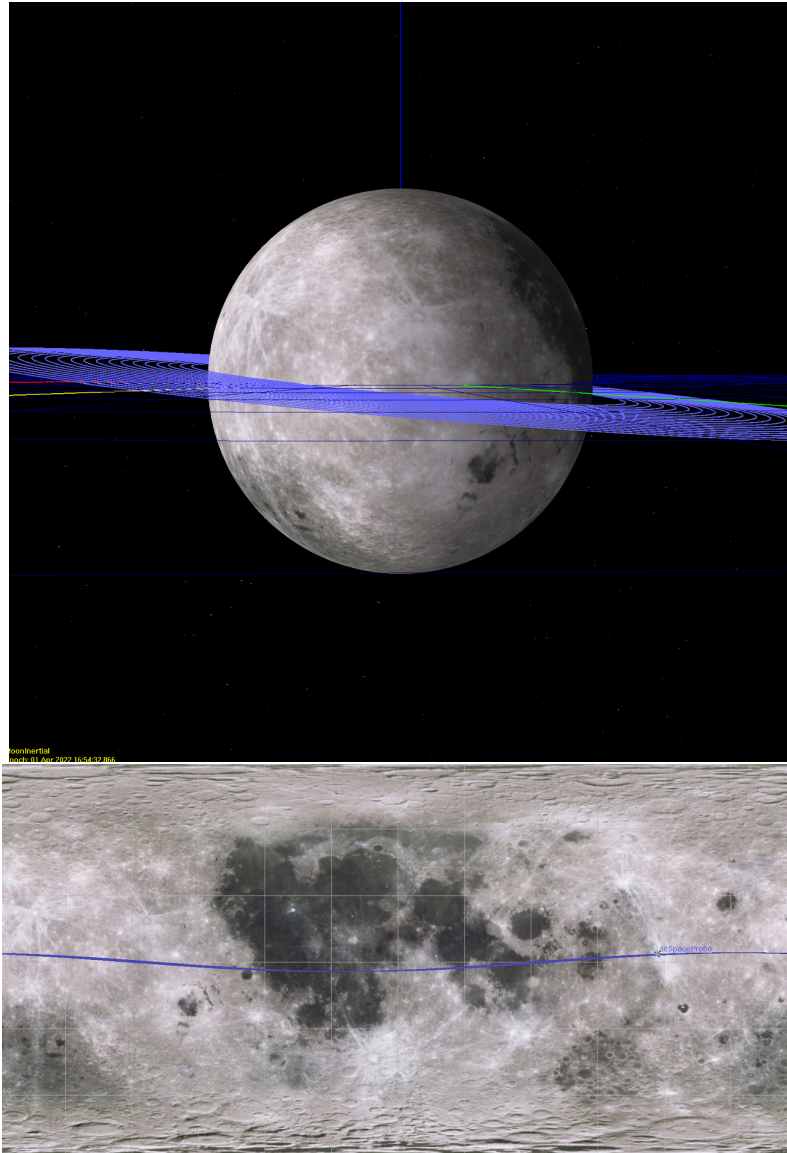**Figure 2.8.** A GMAT simulation visualizing multiple orbits propagated from the same epoch with different initial conditions. The semi-major axis was the only orbital element varied and it is apparent as the circumference of the orbit paths gets larger. The ground tracks for all the orbits are also plotted. This change cannot be seen, however, as the ground tracks cannot physically visualize semi-major axis changes.

2.4   Dynamic Modeling

2.4.1   New Data

While there is an abundance of literature exploring lunar frozen orbits, there is a noticeable lack of comprehensive analysis and results stemming from a full-scale gravity model [60]. As gravitational anomalies are extremely important for lunar orbits at low altitudes, this becomes a major area of interest for future research as parking orbits and lunar hoppers will be an important part of the Artemis plan. Older studies haven't used very accurate gravity fields, however with JPL's Gravity Recovery and Interior Laboratory (GRAIL), the lunar gravity field has been mapped more accurately than ever.

2.4.2   Gravity Potential Derivation

One major focus of this thesis is the orbital perturbation caused by the nonspherical shape of the Moon. In order to properly asses the long-term behavior of a lunar satellite, there must be an accurate description of the gravitational field of the attracting body. Due to the conservative nature of gravity itself, the gravitational field of the Moon can be represented by a potential function. This is usually done by using a mass integral definition and integrating infinitesimal mass elements over the attracting body in order to obtain the potential at a point a fixed distance away [32].
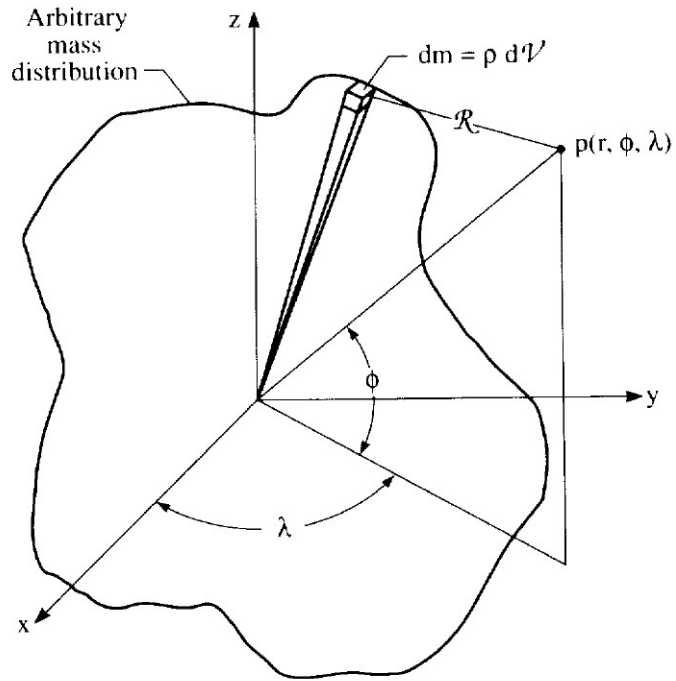
Figure 2.9. Illustration of the parameters being used to derive the potential function from [32]

This potential can be defined as

$$U(r,\phi,\lambda) = \int_{Body} dU = G\int_{Body} \frac{dm}{R} = G\int_{V_{body}} \frac{\rho(r,\phi,\lambda)dV}{R} \tag{2.3}$$

Where:

R defines the distance between the mass element and the exterior point p.

ρ is the density of the body.

V is the volume of the body.

The $\frac{1}{R}$ term can be expanded in a Legendre polynomial series, ultimately resulting in the traditional form of the gravity potential which is defined as:

$$U = \frac{\mu}{r} \left\{ 1 + \sum_{n=2}^{\infty} \sum_{m=0}^{n} \left(\frac{R}{r} \right)^{n} P_{n,m} sin(\phi) \left[C_{n,m} cos(m\lambda) + S_{n,m} sin(m\lambda) \right] \right\} \qquad (2.4)$$

Where:

n declares the degree of the gravity model and m declares the order.

ϕ is the selenocentric latitude of the satellite.

λ is the selenocentric latitude of the satellite.

$P_{n,m}$ is the normalized associated Legendre function of degree n and order m.

$C_{n,m}$ and $S_{n,m}$ are the normalized selenopotential coefficients.

2.4.3   Lunar Gravity Models

The coefficients C_{nm} and S_{nm} are usually determined empirically using tracking satellites orbiting the central body. These values are in turn used to create complete lunar gravity models that define the contributions to the potential field from the non-spherical shape of the Moon [32]. A spherical model is used for the harmonics with the advantage being that it provides a simple analytical approach as the short period effects are averaged out [32]. Additionally, the spherical models are much more accessible and time efficient than mascon models. Mascon models are more appropriate for localized tests and thus a spherical model will suffice for most research. Naturally, the reduction in computation times allows time for optimization routines to achieve the most efficient orbits [32]. There are three types of harmonic coefficients defined by the values of the n and m subscripts. For zonal coefficients, the order m = 0. ($C_{n0} = -J_n$). These coefficients serve to help define the axially symmetric potential of the Moon, which for this scenario happens to be its spin axis [32]. The coefficients are independent of the longitude as they are only defined by the latitude. For a large amount of cases, (including the Earth), this coefficient alone would suffice. However, due to the slow spin of the Moon, the gravity potential is not solely dependent on the zonal terms and the longitudinal considerations must be made. These considerations can be defined by sectorial and tesseral harmonics. For sectorial and tesseral harmonics, the order n = m $\neq$ 0 and the order n $\neq$ m and both $\neq$ 0, respectively. Sectorial harmonics describe the potential along longitudes, placing zero values at the meridians whereas tesseral harmonics describe the potential along both longitudes and latitudes, placing zero values at the parallels of latitude as well [32]. After assignment of the C_{nm} and S_{nm} terms, the individual harmonic terms are superpositioned to completely define the potential.

The physical significance of each of the harmonics can be illustrated by interpreting the coefficients as surface deviations from a perfectly homogeneous sphere. For example, the J_2 term is usually associated with the oblateness, usually seen as an equatorial "bulge". Due to centrifugal force, this oblateness is common among rotating bodies. The C_{22} terms describes

the ellipsoidal shape of the body and the J_3 coefficient describes the triaxial shape of the body, otherwise known as a "pear-like" shape. As the degree of the gravitational terms increases, the description from the gravity potential becomes more localized. The moon has a complex density structure, and thus, requires higher order approximations for accurate results. For zonal harmonics, the degree of the term is correlated to the number of lobes in the equipotential surface [32]. For sectorial and tesseral harmonics, the order represents the number of lobes on a horizontal cross section. The figures below were taken from [32] as they provide a very clear description of how the approximations model the central body.
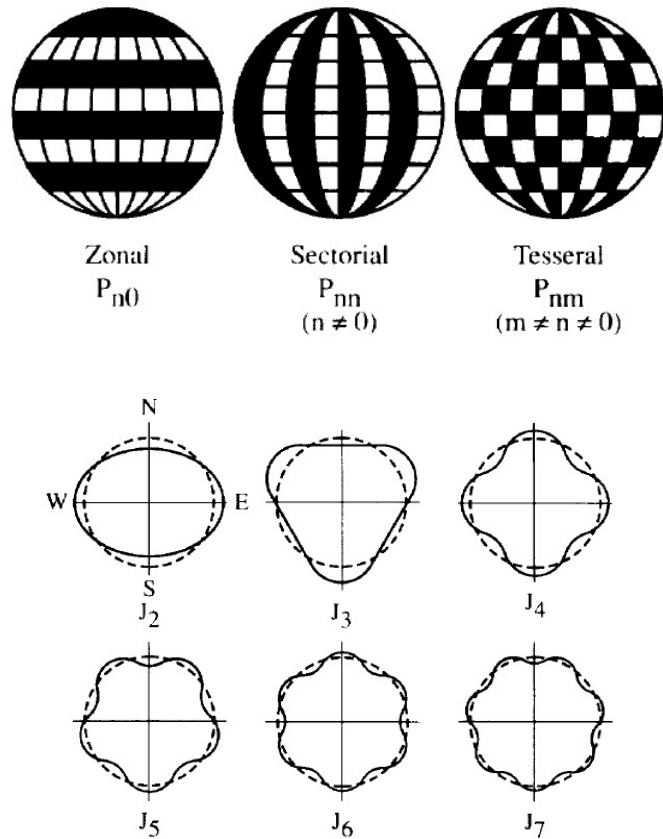
Figure 2.10. Illustration of the Zonal, Sectorial, and Tesseral harmonics. The second figure provides a physical visualization of a few harmonic coefficients with only order increases. Notice the increase in lobes with higher orders.

(a) Harmonic coefficient C_{22}.

(b) Harmonic coefficient C_{33}.
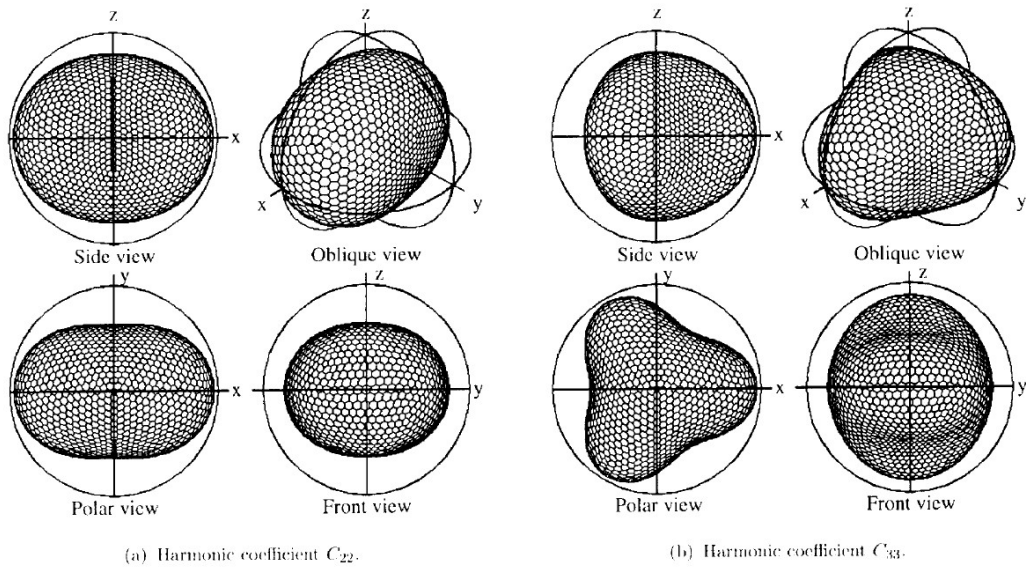
Figure 2.11. Physical visualization of the C_{22} C_{33} bodies.

(a) Harmonic coefficient C_{31}.

(b) Harmonic coefficient C_{54}.

Figure 2.12. Physical visualization of the C_{31} C_{54} bodies.

The values of these gravitational coefficients are calculated through data taken from lunar satellites using radar and laser-ranging to obtain information [32]. Before more modern lunar

27

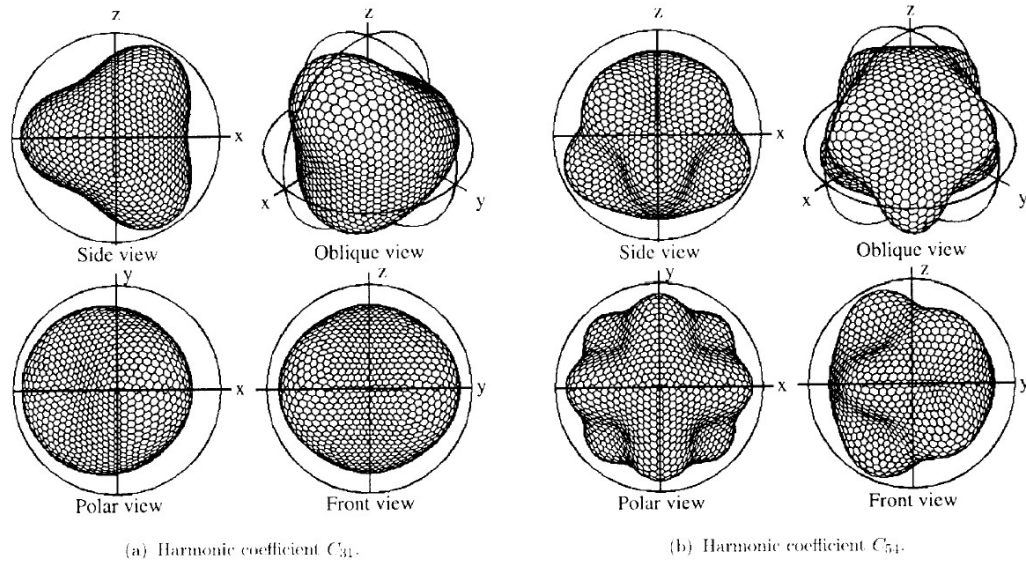missions like GRAIL, there was not a complete model of the gravity field of the Moon. All effects of the lunar gravity field had not been accounted for in the gravity model and only some regions of the Moon had been properly researched. In the present, thanks to recent missions, there are better gravity models available to the public with higher degree and order models of the gravity field. Better instruments and newer technology have also made it possible to accurately assess the gravitational field and calculate more accurate field data as opposed to methods used in the past. Due to limitations of models in the past, papers had not been previously able to properly assess the gravitational potential of the Moon and this thesis seeks to generate new data and both correct and expand on previous results.

2.4.4   Gravity Field Approximations

It should be noted that although the lunar gravity field is quite complex, running calculations at low degrees and orders can still be quite effective in terms of approximating the field and understanding the orbit dynamics. In the case of a lunar low altitude satellites (LLAS) where the gravitational harmonics are most important, many research papers have noticed that including solely the J_2 and C_{22} terms achieves a good approximation of the field and have minor differences between their higher degree and order counterparts. [8, 9, 32, 53, 60–62]. In most cases, terms can be applied when they directly affect the parameters being researched. (Meyer 1994) looks at lifetimes of lunar orbits and includes the J_5 term in their model as it contributes the most to altitude decay in a LLAS. (De Saedeleer 2006 and Tzriti 2010) noticed that the inclusion of the C_{22} is necessary for most orbits as it directly plays a part in the parameters of a frozen orbit as it affects the critical inclination. (Tzirti 2010) notes that 3rd degree gravity harmonics are important in the long term stability of the orbit as it causes chaotic regions to appear as well as significant changes in the secular behavior of the orbit. The 3rd degree lunar gravity terms are most important at an altitude above 2000 km. (Carvalho 2006 and Tzirti 2010) note that the J_5 and C_{31} terms are also noticeable to LLAS as they noticeably change the variation of eccentricity and directly affect the lifetime of the orbit. If one uses solely first and second order, the variation of e over time is not

Gravitational Harmonic Coefficients				
Harmonic Co-efficients	Eccentricity	Inclination	Ascending Node	Argument of Periapsis
J_2	No	No	Yes	Yes
J_3	Yes	No	No	No
J_5	Yes	No	No	No
C_{22}	No	Yes	Yes	Yes
C_{31}	Yes	No	No	Yes

present [62]. The J_3 term (parllactic) changes the eccentricity of a circular orbit and may cause large variations if the orbit is sufficiently large [61]. (Carvalho 2010) notes that for LLAS in the polar regions, the J_2 and C_{22} terms dominate and are of utmost importance. (Singh 2020) notes that an increase in the degree of the gravity model does not affect ω significantly, and thus it is not necessary if that orbital element is of interest. However, it is noted that the variation of the degree causes significant changes in the prediction accuracy of the apoapsis and periapsis altitudes [60]. The paper also notes that with more elliptical orbits, the variation in altitude accuracy becomes less significant and eventually converges [60]. In contrast to a 50x50 or higher gravity field, these approximations save time and allow for more efficient analysis and perhaps better solutions.

2.4.5   Time Scale Dependency

Time scales are also an important factor for proper orbit analysis. Each of the orbital elements display different behavior and oscillates throughout time with different periods. In order to properly understand the evolution, changes must be recorded, and oscillations secularized at proper time scales. For third body considerations, the long period motion should be fairly long in comparison to the period of the disturbing body [61]. The semi-major axis and men motion of a lunar satellite are usually constant in long period motion and do not need to be considered when selecting the proper harmonics. e has long period variations, usually in the realm of years [9]. The inclination on the other hand is characterized by large medium-period variations [9]. ω and Ω have secular drifts that are larger than the periodic variations [9]. These variations will be

present or absent depending on the harmonics used so it is important to take into consideration which evolutions will be important for the orbit at hand.

2.4.6 Initial Condition Dependency

The initial conditions of an orbit are also of vital importance to the not only the validity but the evolution of an orbit as well [32]. Differing initial conditions can cause large variations in the oscillation of orbital elements and ultimately affect the lifetime of the orbit itself. It is necessary to have longer orbit lifetimes for both tracking and intermediary transfer purposes [32]. For example, lunar satellites with inclined orbits of more than 39.23 degrees with respect to the Earth's orbital lane experience considerable growth of eccentricity [62]. This can be attributed to the Earth causing a Kozai resonance causing the eccentricity to grow [62]. In general, the Earth's eccentricity and inclination have a vital influence on the variation of the inclination and eccentricity of the satellite itself. Another example involves the critical semi-major axis, which is the region where the perturbations of J_2, C_{22}, and 3rd body have the same magnitude. The location of the critical semi-major axis is entirely dependent on the longitude of the ascending node [62]. When using 2nd order theory, the eccentricity is directly affected by the initial inclination. (Carvalho 2010) shows a slow increase in temporal variation of eccentricity in satellites with larger inclinations. Additionally, as more and more gravity harmonic terms are considered, the orbital element variations become increasingly sensitive to the initial conditions [62].

2.4.7 Critical Inclination

Another parameter to consider in terms of both initial conditions and frozen orbits is the critical inclination. The critical inclination describes the inclination at which there is zero apogee drift for an elliptical orbit. (Orlov 1954) was the first to notice interesting orbit behavior at a certain inclination and the classical critical inclination was found by (Szebehely 1989) and is 63.26. The critical inclination depends on a variety of factors including the which gravitational

harmonics are being used for the gravity field and which force models are used along with the argument of periapsis and ascending node. (De Saedeleer 2006) showed that when the C_{22} term is considered, the critical inclination becomes 39.14 regardless of initial conditions, whereas for solely J_2, the critical inclination is the classic value [53]. The orbit behaves differently based on where its inclination is situated relative to the critical inclination. Below the critical inclination, small eccentricities produce small amplitudes of variations, whereas above the critical inclination, the same can be said for highly eccentric orbits [62]. The argument of periapsis liberates when the initial inclination is higher than critical and circulates when lower [62]. The properties of critical inclinations are not set in stone nor are they high fidelity. In reality, the time evolution of the inclination causes variations in the argument of periapsis, in which the term critical inclination is no longer valid. As a work around, (Tzirti 2010) uses a quasi-critical inclination instead for solution in which the argument of pericenter liberates. It should also be noted that these dynamics are also highly dampened when the rotation of the moon is taken into account and motion returns to regular [8, 53].

2.4.8 Areas for Errors

All of the aforementioned theory is essential to the accurate modeling of lunar orbits. In order to properly use approximation, there must be a deep understanding of the lunar environment. Although the variation of orbital elements for one revolution may be small, there is certainly a compounding effect as time progresses if left unchecked. The size of the errors calculated with approximations can be estimated from the magnitudes of the quantities that were ignored during the development of said formulas [10]. The errors also grow as the distance from the central body increases. For moon satellite orbits, the basic factor determining the error in the approximation is the largest value of the perturbing acceleration and the long revolution periods resulting from calculating only the first approximation in the motion of the perturbing body [10]. When accounted for, the errors can be dissipated and approximation methods can be used for a wide range of satellite orbits [10].

2.4.9   Third Body Considerations

As mentioned previously, the Earth plays a role in the behavior and parameters of a lunar satellite orbit as well. However, unlike gravitational harmonics, the third body effects from the Earth are negligible at low altitudes. Said third body effects become noticeable around a semi-major axis of 3000km and above, defining the range of lunar high altitude satellites (LHAS) [53]. From an semi-major axis of 3000km all the way to the hill sphere of the Moon, the third body effects from the earth can no longer be ignored and become more and more apparent, causing stronger instabilities and instilling chaotic regions for some orbit inclinations [8, 53]. At a distance 4000km from the Moon, the Earth's perturbing effect is much greater than those of harmonic and solar causes [14]. The Earth's perturbing effect becomes of the order of 1/10 of the central acceleration [14]. At this point, an orbit would likely not be stable and would be grossly disturbed. Finally, the Moon has a hill radius of 58,000 km, at which the Earth's gravitational forces eventually take over. In general, adding Earth third body effects creates larger variations in the inclination amplitude and frequency [8]. Third body effects also have the greatest effect on eccentricity for initial eccentricities around 0.707 and high inclination satellite orbits. They are dependent on the average value of ω as well [32]. Earth third body effects also play an important role in the lifetimes of lunar orbits as they change the eccentricity and can cause premature crashes.

2.4.10   Sun Synchronous Lunar Orbits

For the ARTEMIS lunar missions, a particular area of interest is the possibility of a Lunar Sun Synchronous Orbit (LSSO). An LSSO would provide an invaluable asset to not only the current ARTEMIS missions, but future missions as well. Due to its nature as a LSSO, the entirely of the moon could be imaged with proper illumination. The images could provide an updated visual database of the dark side of Moon and support new research on the selenography. The satellite could provide essential selenographical information and tracking services for all

32

ground-based operations. In order to achieve this, the satellite would have to precess so that it's Ω is always situated on the vector pointing to the sun.

Looking at the figures, it is clear to see that the physically possible orbits are unable to achieve the necessary nodal precession even remotely. Although the rates are calculated from analytic theory, it is not necessary to run simulations to replicate this result as the values are not close enough to motivate further study. Since the gravity harmonics and 3rd body perturbations cannot alone provide the necessary satellite nodal precession, taking advantage of solar radiation pressure may be an option. A proper area to mass ratio could perhaps give the push needed to reach the necessary value for nodal precession. A satellite which aims to maximize this ratio is known as a high area-to-mass ratio (HAMR) object.

Chapter 3

Results and Discusion

The results are presented in an "atlas" of dynamical stability maps for different orbital regions of interest. GMAT simulations were run for a grid of initial conditions of Ω and inclination. A meshgrid containing inclination = [0:6:180] and Ω = [0:12:360] was used for all of the following. The first three plots were done for the J_2 perturbation effect.
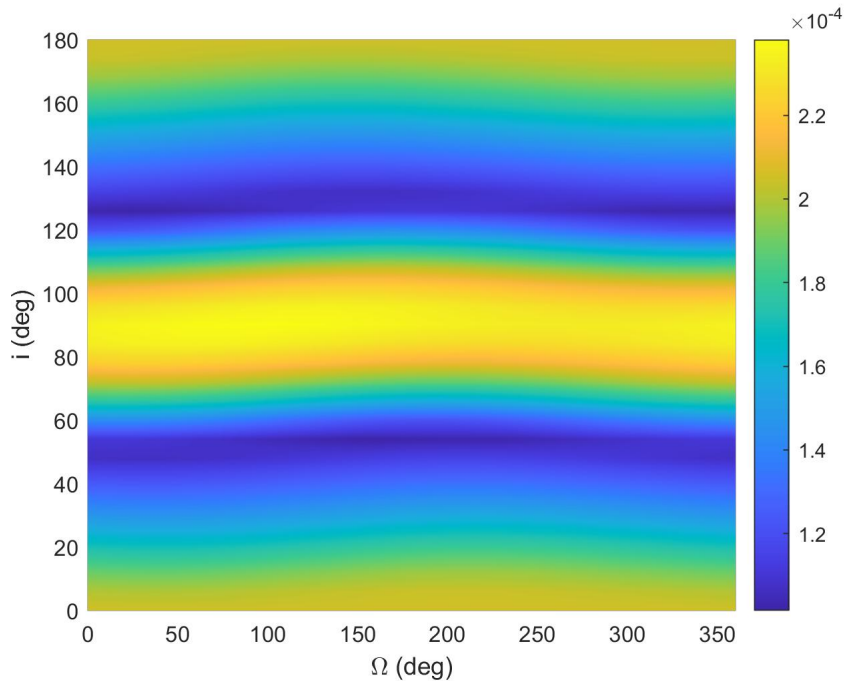

Figure 3.1. A phase space graph of the eccentricity perturbations caused by the J_2 effect. The initial conditions used were [a, e, i, Ω, ω, v] = [2000, 0.05, 0-180, 0-360, 45, 0]. The orbit was simulated for a period of 30 days.

The semi-major axis of 2000km was chosen are gravitational harmonics are much more noticeable closer to the central body's surface. The eccentricity was chosen to simulate a near circular orbit as most parking orbits close to the surface are of this nature. The argument of periapsis and mean anomaly are arbitrary. As expected, since the oblateness coefficient is not theoretically responsible for changes in the eccentricity, the magnitude of the perturbations are virtually 0.
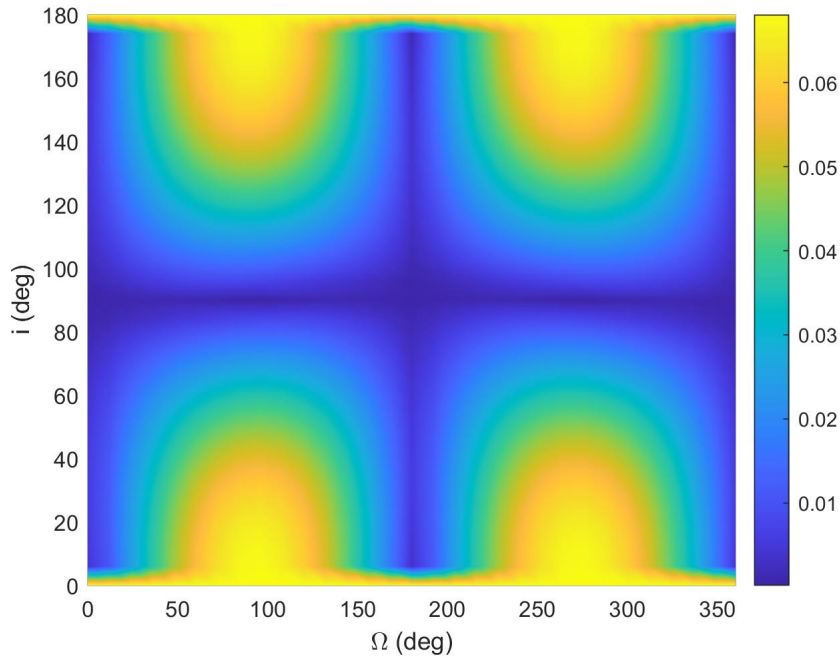

Figure 3.2. A phase space graph of the inclination perturbations caused by the J_2 effect after a period of 30 days. The initial conditions used were [a, e, i, Ω, ω, ν] = [2000, 0.05, 0-180, 0-360, 45, 0].

There are some very small, although noticeable changes in the inclination, with most occurring at the equator around Ω values of 90 degrees and 270 degrees. From the literature, this is expected as the oblateness does not directly affect the inclination.
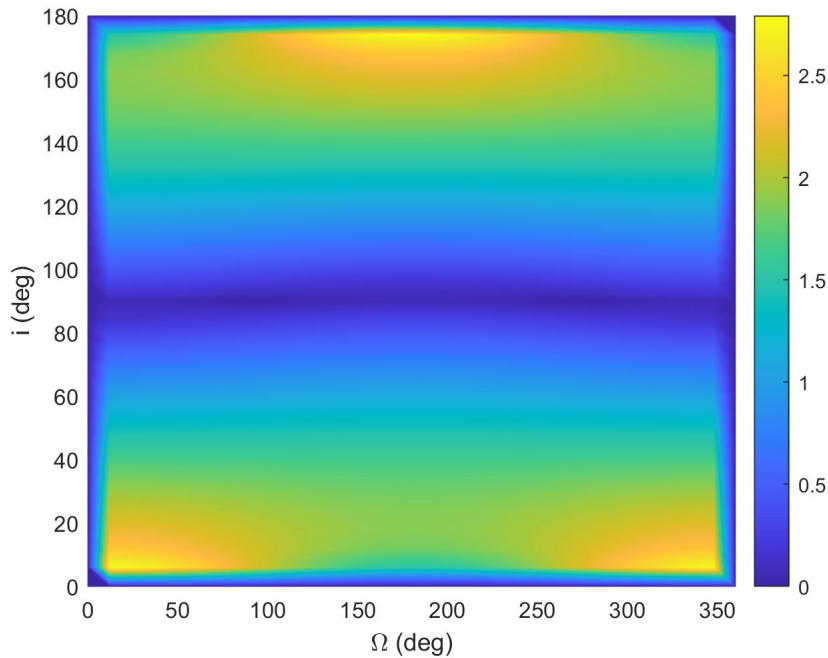
Figure 3.3. A phase space graph of the ascending node perturbations caused by the J_2 effect after a period of 30 days. The initial conditions used were [a, e, i, Ω, ω, v] = [2000, 0.05, 0-180, 0-360, 45, 0].

As expected, the J_2 coefficient has a direct effect on the ascending node. According to the analytical solution, which has a cosine term being a function of inclination, the perturbations should be cancelled around inclinations of 90 degrees. This certainly holds true as there are no perturbations around that area. The highest perturbations seem to occur around inclination at the equator and ascending node values of 360 and 180 degrees. Note that the borders of the phase space are all 0. This was done post processing as GMAT was returning unrealistic values, which in turn was causing an unscaled phase space map. The next group of plots were done for the C_{22} perturbations.
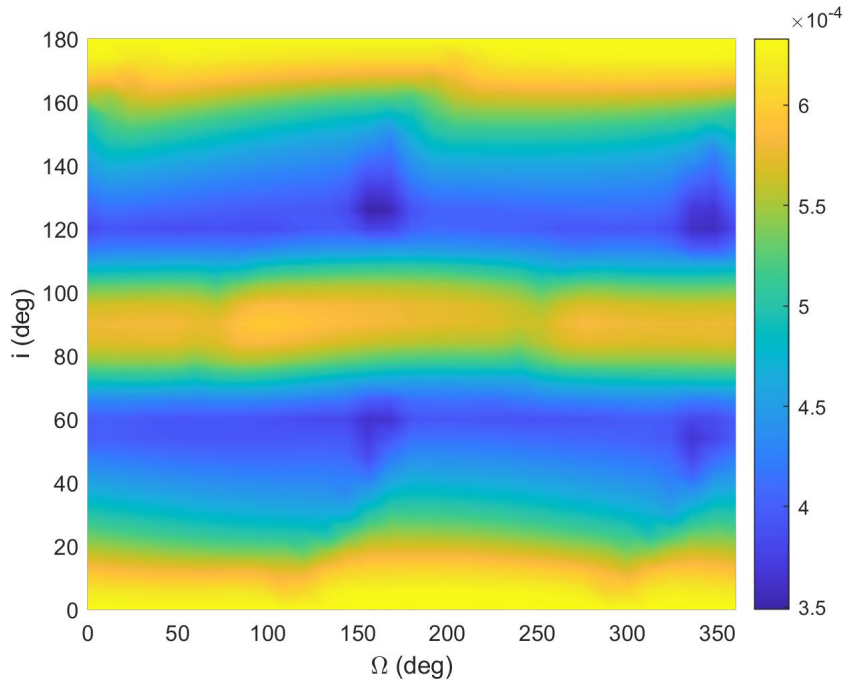
Figure 3.4. A phase space graph of the eccentricity perturbations caused by the C_{22} gravity harmonics after a period of 30 days. The initial conditions used were [a, e, i, Ω, ω, v] = [2000, 0.05, 0-180, 0-360, 45, 0].

Once again, as expected, the gravity harmonics cause negligible changes in the eccentricity and not important with the low orders and degrees. However, it will be see later in the paper that there exists a certain point in the approximation of the gravity field at which eccentricity changes become apparent and can no longer be ignored over longer periods of time.
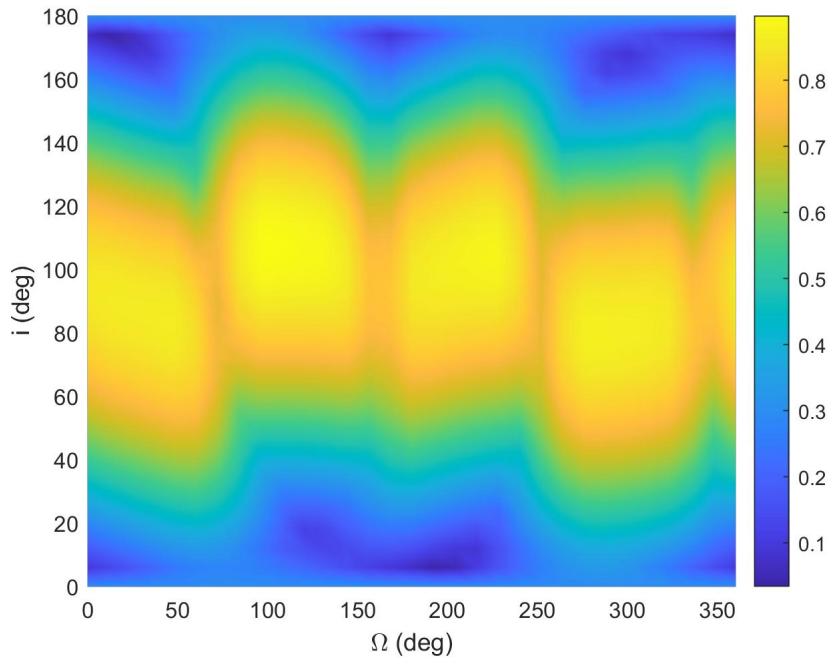
Figure 3.5. A phase space graph of the inclination perturbations caused by the C_{22} gravity harmonics after a period of 30 days. The initial conditions used were [a, e, i, Ω, ω, v] = [2000, 0.05, 0-180, 0-360, 45, 0].

Unlike the J_2 harmonics, those of C_{22} have a noticeable effect on the inclination. This was predicted by theory as well. The biggest changes seem to occur around the range of 60 degrees and 120 degrees. The inclination changes are large enough to warrant exponential changes due to gravity effects in the long run.
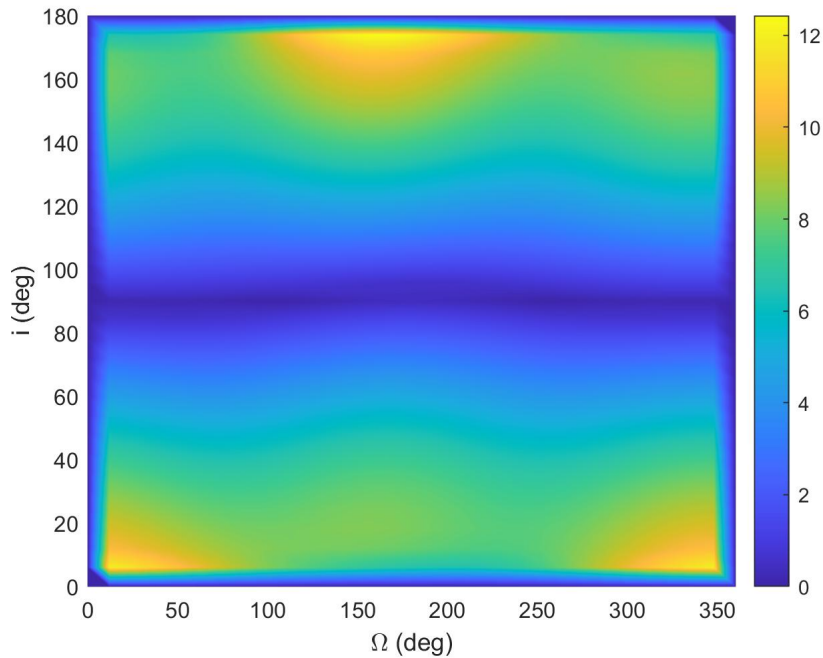
Figure 3.6. A phase space graph of the ascending node perturbations caused by the C_{22} gravity harmonics after a period of 30 days. The initial conditions used were [a, e, i, Ω, ω, v] = [2000, 0.05, 0-180, 0-360, 45, 0].

As expected from the theory, there are changes to be expected caused by the C_{22} harmonics. Similar to those of J_2, the biggest changes occur around inclinations of 0 degrees and 180 degrees and ascending nodes of 260 degrees. Unlike the J_2 perturbations, however, the C_{22} harmonics create massive changes to the ascending node over the period of 30 days. The next group contains plots from Earth third body effects.
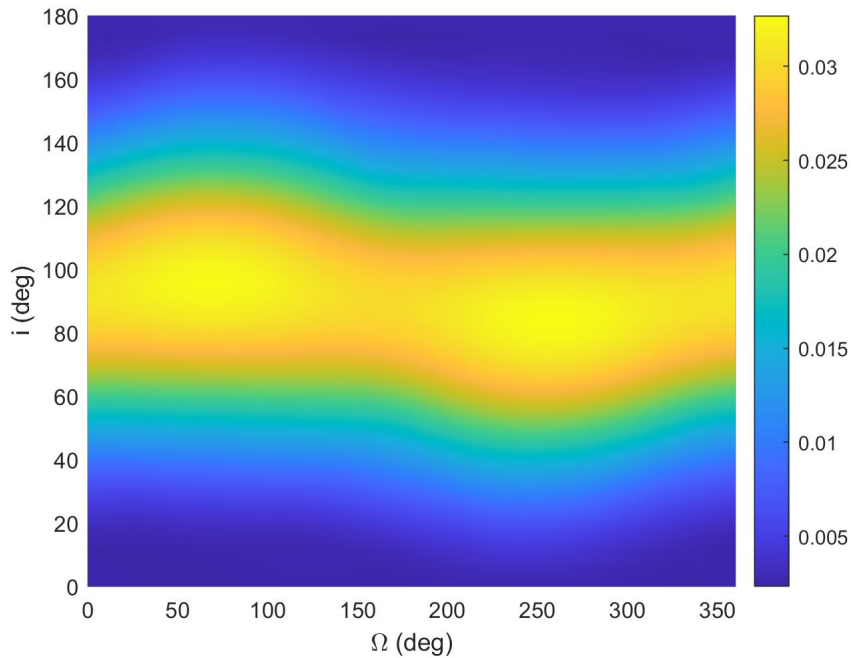
Figure 3.7. A phase space graph of the eccentricity perturbations caused by the Earth third body effects after a period of 30 days. The initial conditions used were [a, e, i, Ω, ω, ν] = [4000, 0.05, 0-180, 0-360, 45, 0]. Unlike the initial conditions for the gravity harmonics, a semi-major axis of 4000km was used. Since third body perturbations are almost negligible in comparison to those of the gravity harmonics at low altitudes, a higher altitude was chosen. Papers such as [14] and [8] state that Earth third body effects begin to dominate the gravity harmonics around 4000km. For this reason, that exact semi-major axis was chosen.

As expected from the theory, third body effects are directly responsible for eccentricity changes, and in turn, for the lifetimes of orbits. It can be confidently predicted that as the semi-major axis initial condition were increased, the perturbations would grow exponentially. As the theory predicts, chaotic regions would eventually appear, making the orbit extremely unstable.
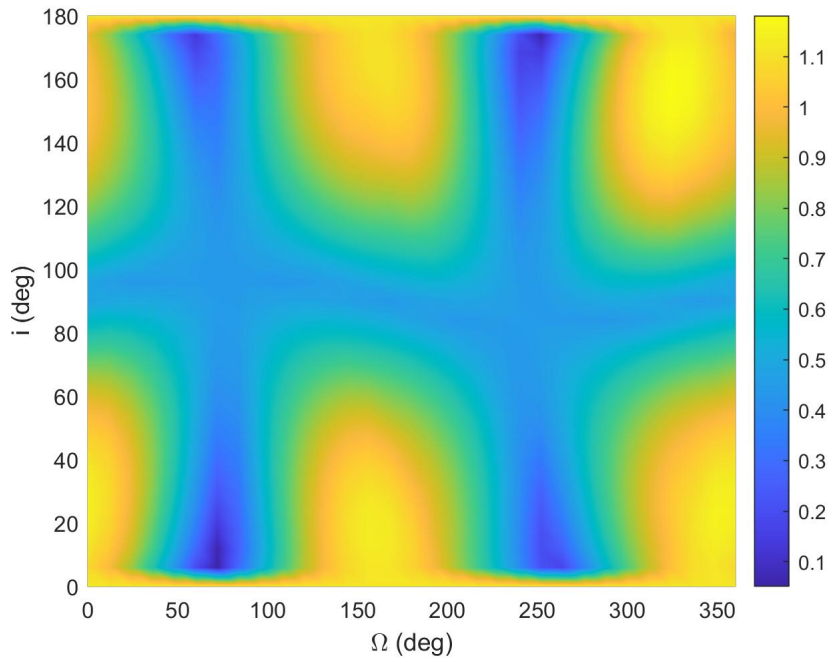
Figure 3.8. A phase space graph of the inclination perturbations caused by the Earth third body effects after a period of 30 days. The initial conditions used were [a, e, i, Ω, ω, ν] = [4000, 0.05, 0-180, 0-360, 45, 0].

As expected, Earth third body effects do have a noticeable effect on the inclination. The behavior is similar to that of the J_2 effect where there are "ovals" in the phase space where the biggest magnitudes occur. For this particular case, the biggest magnitudes occur at inclinations around the equator and ascending nodes at values of 180 degrees and 360 degrees. The magnitudes themselves should warrant attention and will only get bigger with an increase in the semi-major axis, ultimately leading to unstable properties.
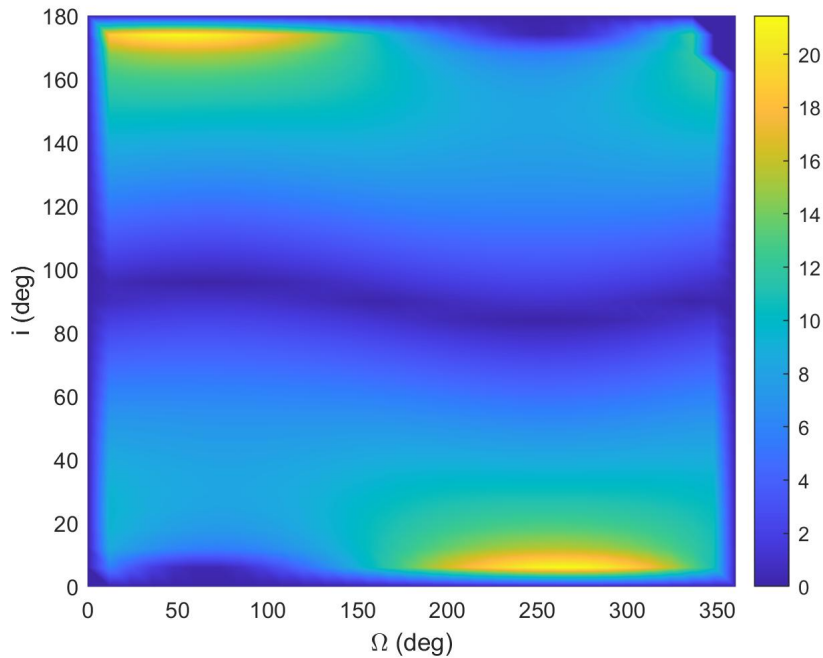
Figure 3.9. A phase space graph of the ascending node perturbations caused by the Earth third body effects after a period of 30 days. The initial conditions used were [a, e, i, Ω, ω, ν] = [4000, 0.05, 0-180, 0-360, 45, 0].

There are two hot-spots where large changes occur at the equator at ascending node values of 0 degrees and 270 degrees. At an inclination of 90 degrees, there no ascending node perturbations and most of phase has relatively minimal values. Similar to previous results, the boundaries are zeroed out. The next group of plots were done for a high fidelity 64x64 gravity field.
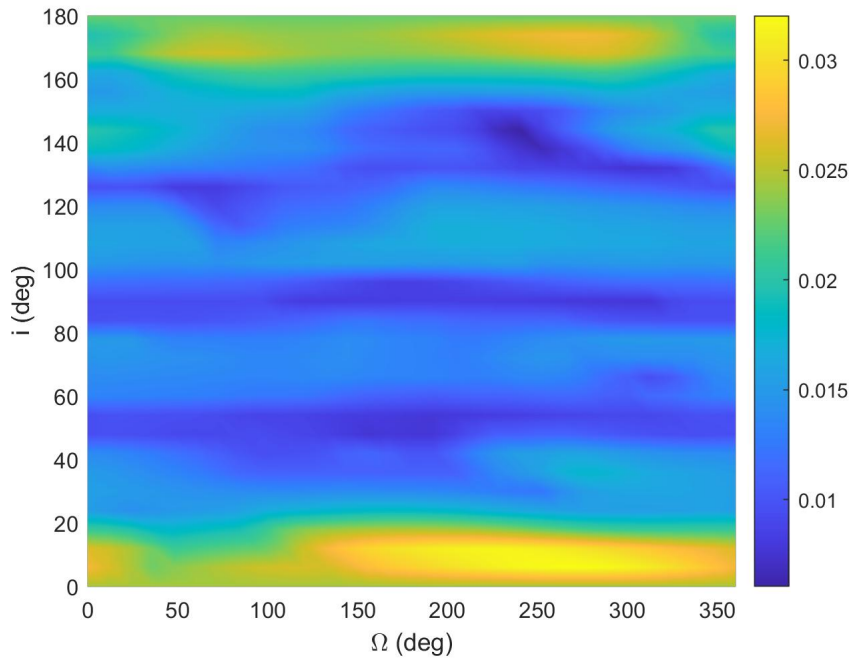
Figure 3.10. A phase space graph of the eccentricity perturbations caused by gravity harmonic effects after a period of 30 days. For this case, a large 64x64 degree and order expansion was used to obtain a detailed map of the gravity harmonics. The initial conditions used were [a, e, i, Ω, ω, v] = [2000, 0.05, 0-180, 0-360, 45, 0].

Similar to the previous gravity harmonic phase spaces, the semi-major axis for this space was 2000km to be able to measure the full effect close to the surface. Unlike the previous two, however, there are noticeable changes in eccentricity for this case. The biggest magnitudes occur at on a prograde equatorial orbit. Although there are relatively large perturbations for the whole equatorial range, the biggest occur between initial ascending nodes of 160 degrees and 340 degrees.
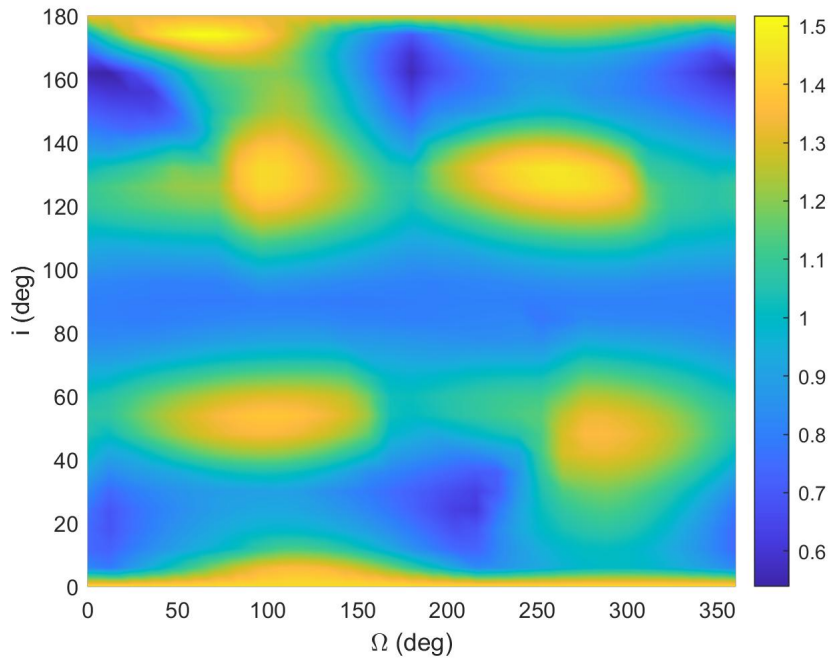
Figure 3.11. A phase space graph of the inclination perturbations caused by gravity harmonic effects after a period of 30 days. For this case, a large 64x64 degree and order expansion was used to obtain a detailed map of the gravity harmonics. The initial conditions used were [a, e, i, Ω, ω, v] = [2000, 0.05, 0-180, 0-360, 45, 0].

Similar to previous cases dealing with inclination, there are noticeable inclination increases which occur in oval-like shapes. There are a greater number of these regions and they occur around ascending nodes of 100 degrees and 290 degrees. For the inclinations, these regions occur at the equator and at inclinations of 50 degrees and 130 degrees. There are also greater magnitude of inclination changes than the previous cases.
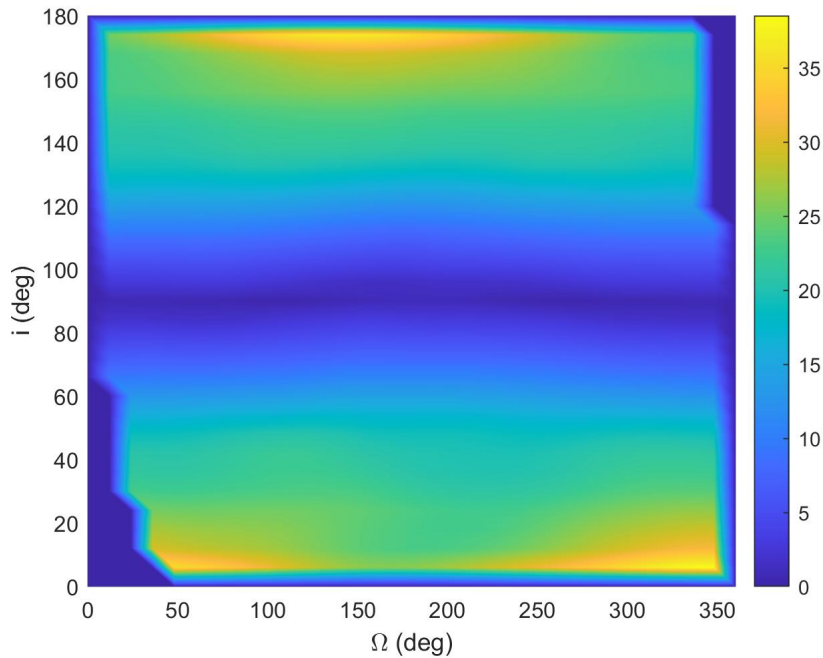
Figure 3.12. A phase space graph of the ascending node perturbations caused by gravity harmonic effects after a period of 30 days. For this case, a large 64x64 degree and order expansion was used to obtain a detailed map of the gravity harmonics. The initial conditions used were [a, e, i, Ω, ω, ν] = [2000, 0.05, 0-180, 0-360, 45, 0].

In this case, the perturbations look to be the greatest in similar areas as the previous runs. In comparison to previous cases, the perturbations are much greater and magnitude and could be in consideration for building an LSSO. The boundaries are zeroed out as well as certain regions exhibiting unrealistic values. The next group of plots investigate the combined effect of a 64x64 field along with Earth third body effects.
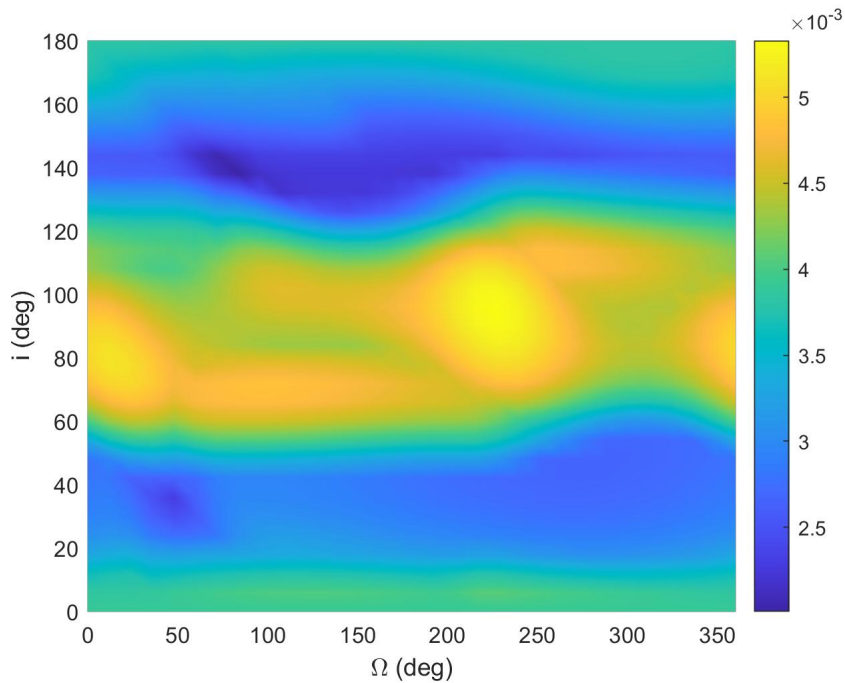
Figure 3.13. A phase space graph of the eccentricity perturbations caused by gravity harmonic effects as well as Earth third body effects after a period of 30 days. For this case, a large 64x64 degree and order expansion was used to obtain a detailed map of the gravity harmonics. Additionally, Earth third body effects were taken into consideration. The initial conditions used were [a, e, i, Ω, ω, ν] = [3000, 0.05, 0-180, 0-360, 45, 0].

This time, the semi-major axis has a value of 3000km which was chosen as the average from both types of perturbations so the satellite would have an altitude where both types are apparent. Interestingly, however, in this case the perturbations are nearly negligible. Most occurs at inclinations of 90 degrees which can be most likely attributed due to Earth third body effects.

Figure 3.14. A phase space graph of the inclination perturbations caused by gravity harmonic effects as well as Earth third body effects after a period of 30 days. For this case, a large 64x64 degree and order expansion was used to obtain a detailed map of the gravity harmonics. Additionally, Earth third body effects were taken into consideration. The initial conditions used were [a, e, i, Ω, ω, ν] = [3000, 0.05, 0-180, 0-360, 45, 0].

There are noticeable inclinations perturbations for nearly the entire map, with the more stable area being around the equator. It would be important to keep these changes in mind as over long periods of time, these changes will only intensify and ultimately accumulate into large changes in the orbit shape. This, as has been noted earlier in the paper, will cause increasing areas of instability.
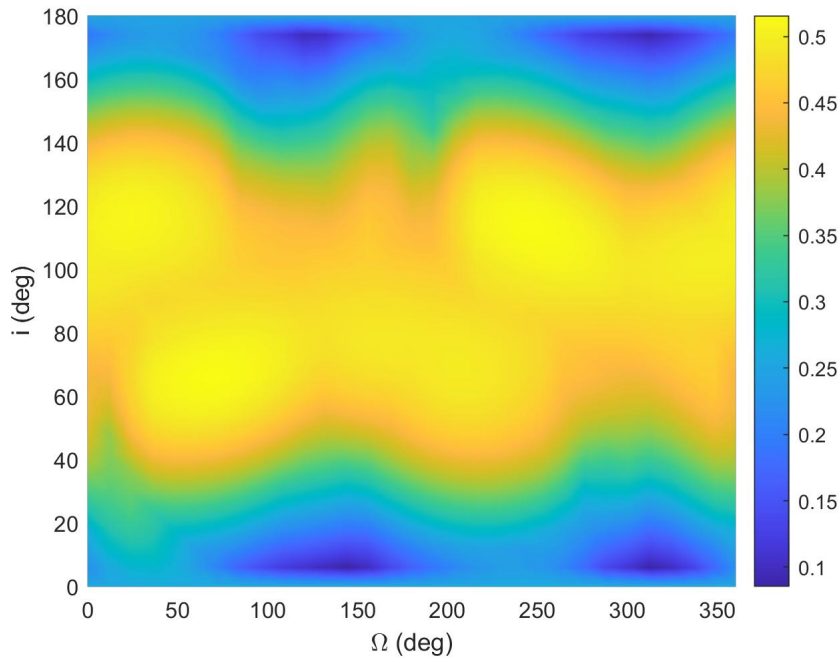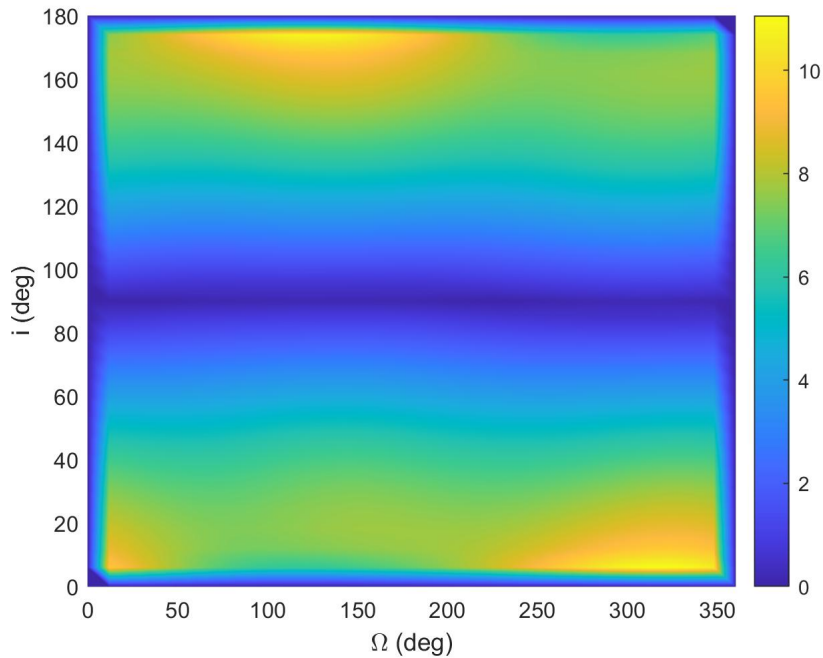
Figure 3.15. A phase space graph of the ascending node perturbations caused by gravity harmonic effects as well as Earth third body effects after a period of 30 days. For this case, a large 64x64 degree and order expansion was used to obtain a detailed map of the gravity harmonics. Additionally, Earth third body effects were taken into consideration. The initial conditions used were [a, e, i, Ω, ω, ν] = [3000, 0.05, 0-180, 0-360, 45, 0].

Similar to previous cases, the inclination of 90 degrees looks to be an area for equilibrium. However, differently from those previous cases, the biggest magnitudes occur at the equator at initial ascending nodes of 150 degrees and 360 degrees. This can most likely be attributed to the part Earth third body effects play on creating different chaotic regions from the solely harmonic case.

Chapter 4

Conclusions and Future Work

Long-term orbiter lifetimes will be an important factor in the efficacy of future human habitation of the Moon. Throughout the thesis, it has been clear that optimizing these lifetimes will require meticulous calculation of orbital perturbations and proper selection of orbital initial conditions. After comparison of the simulations with predicted models from the literature, most of the results agree with what has been calculated analytically. The dynamic stability charts indicate higher magnitudes of perturbations for the corresponding perturbing forces and orbital elements than previously thought. Possibly some of the most important results are those from the C22, 64X64, and 64x64 + Third Body runs. The C22 run verifies the higher order gravitational anomaly existence and cements the need for more robust models. The 64x64 run does more of the same, and gives an approximation of the sheer magnitudes of perturbations that can be felt. The 64x64 + Third Body case shows how the combination of the dynamics can ultimately result in a destructive effect in the magnitude of perturbations. It should be noted that the orbital space studied in particulate produced destructive properties with the summation of different models, and that a large amount of orbits will display dangerously constructive properties. This work can certainly be expanded upon further.The test case simulations run are only a fraction of all possible cases. The Earth third body cases can be run at higher altitudes, where their forces may be more present. The simulations could be run for longer periods of time, where one would be able to notice their behavior develop along longer portions of time. Sun-synchronous orbits

could also be explored further with GMAT runs exploring differing precessions due to varying realistic area-to-mass ratios. There is certainly room for improvement and further exploration in the case of lunar orbiters.

Bibliography

[1] J. d. S. Carvalho, R. Vilhena de Moraes, and A. Prado, "Some orbital characteristics of lunar artificial satellites," *Celestial Mechanics and Dynamical Astronomy*, vol. 108, no. 4, pp. 371–388, 2010.

[2] E. Belbruno and J. Miller, "Sun-perturbed Earth-to-Moon transfers with ballistic capture," *Journal of Guidance, Control, and Dynamics*, vol. 16, pp. 770–775, 1993.

[3] W. Koon, M. Lo, J. Marsden, and S. Ross, "Low-energy transfer to the Moon," *Celestial Mechanics and Dynamical Astronomy*, vol. 81, pp. 63–73, 2001.

[4] T. Sweetser, S. Broschart, V. Angelopoulos, and Others, "ARTEMIS mission design," *Space Science Reviews*, vol. 165, pp. 27–57, 2011.

[5] L. Zhang, "Development and prospect of Chinese lunar relay communication satellite," *Space: Science & Technology*, vol. 2021, p. 3471608 (14 pp.), 2021.

[6] D. Steichen, "An averaging method to study the motion of lunar artificial satellites I. Disturbing function," *Celestial Mechanics and Dynamical Astronomy*, vol. 68, pp. 205–224, 1998.

[7] D. Steichen, "An averaging method to study the motion of lunar artificial satellites II. Averaging and applications," *Celestial Mechanics and Dynamical Astronomy*, vol. 68, pp. 225–247, 1998.

[8] B. De Saedeleer, "Analytical theory of a lunar artificial satellite with third body perturbations," *Celestial Mechanics and Dynamical Astronomy*, vol. 95, pp. 407–423, 2006.

[9] T. Nie and P. Gurfil, "Lunar frozen orbits revisited," *Celestial Mechanics and Dynamical Astronomy*, vol. 130, p. 61 (35 pp.), 2018.

[10] Y. Kozai, "Motion of a lunar orbiter," *Publications of the Astronomical Society of Japan*, vol. 15, pp. 301–312, 1963.

[11] C. Oesterwinter, "Motion of a lunar satellite," *The Astronomical Journal*, vol. 71, pp. 987–

989, 1966.

[12] S. Hamid, "The force function on a lunar satellite due to the oblateness of the Moon," *Smithsonian Astrophysical Observatory Special Report*, vol. 236, pp. 221–246, 1966.

[13] T. L. Felsentreger, "Classification of lunar satellite orbits," *Planetary and Space Science*, vol. 16, pp. 285–295, 1971.

[14] A. Roy, "The theory of the motion of an artificial lunar satellite I. Development of the disturbing function," *Icarus*, vol. 9, pp. 82–132, 1968.

[15] A. Roy, "The theory of the motion of an artificial lunar satellite II. The first-order and second-order theories," *Icarus*, vol. 9, pp. 133–161, 1968.

[16] C. Oesterwinter, "The motion of a lunar satellite," *Celestial Mechanics*, vol. 1, pp. 368–436, 1970.

[17] G. Giacaglia, J. Murphy, and T. L. Felsentreger, "A semi-analytic theory for the motion of a lunar satellite," *Celestial Mechanics*, vol. 3, pp. 3–66, 1970.

[18] V. Brumberg, L. Evdokimova, and N. Kochina, "Analytical methods for the orbits of artificial satellites of the Moon," *Celestial Mechanics*, vol. 3, pp. 197–221, 1971.

[19] K. Meyer, J. Buglia, and P. Desai, "Lifetimes of lunar satellite orbits," 1994. NASA Technical Paper 3394.

[20] P. d'Avanzo, P. Teofilatto, and C. Ulivieri, "Long-term effects on lunar orbiter," *Acta Astronautica*, vol. 40, pp. 13–40, 1997.

[21] M. Lara, "Design of long-lifetime lunar orbits: A hybrid approach," *Acta Astronautica*, vol. 69, pp. 186–199, 2011.

[22] S. Gupta and R. Sharma, "Effect of altitude, right ascension of ascending node and inclination on lifetime of circular lunar orbits," *International Journal of Astronomy and Astrophysics*, vol. 1, pp. 155–163, 2011.

[23] S. Tzirti, A. Noullez, and K. Tsiganis, "Secular dynamics of a lunar orbiter: a global exploration using Prony's frequency analysis," *Celestial Mechanics and Dynamical Astronomy*, vol. 118, pp. 379–397, 2014.

[24] J. San-Juan, R. López, and I. Pérez, "High-fidelity semianalytical theory for a low lunar orbit," *Journal of Guidance, Control, and Dynamics*, vol. 42, pp. 161–165, 2019.

[25] S. McArdle and R. Russell, "Circulating, eccentric periodic orbits at the Moon," *Celestial*

Mechanics and Dynamical Astronomy, vol. 133, p. 18 (27 pp.), 2021.

[26] A. Tselousova, S. Trofimov, and M. Shirobokov, "Station-keeping in high near-circular polar orbits around the Moon," *Acta Astronautica*, vol. 188, pp. 185–192, 2021.

[27] C. A. Kluever, *Space flight dynamics*. John Wiley & Sons, 2018.

[28] R. H. Battin, *An Introduction to the Mathematics and Methods of Astrodynamics*. Reston: American Institute of Aeronautics and Astronautics, Rev. ed., 1999.

[29] D. J. Scheeres, *Orbital Motion in Strongly Perturbed Environments: Applications to Asteroid, Comet and Planetary Satellite Orbiters*. Berlin: Springer-Praxis, 2012.

[30] A. J. Rosengren and D. J. Scheeres, "On the Milankovitch orbital elements for perturbed Keplerian motion," *Celestial Mechanics and Dynamical Astronomy*, vol. 118, pp. 197–220, 2014.

[31] W. A. Rahoma and F. A. Abd El-Salam, "The effects of moon's uneven mass distribution on the critical inclinations of a lunar orbiter," *Journal of Astronomy and Space Sciences*, vol. 31, no. 4, pp. 285–294, 2014.

[32] K. W. Meyer, J. J. Buglia, and P. N. Desai, *Lifetimes of lunar satellite orbits*, vol. 3394. National Aeronautics and Space Administration, Langley Research Center, 1994.

[33] A. E. Roy, *Orbital Motion*. New York: Taylor & Francis, 4 ed., 2005.

[34] D. Scheeres, "The restricted hill four-body problem with applications to the earth–moon–sun system," *Celestial Mechanics and Dynamical Astronomy*, vol. 70, no. 2, pp. 75–98, 1998.

[35] L. Liu and J.-s. Wang, "An analytic solution of the orbital variation of lunar satellites," *Chinese Astronomy and Astrophysics*, vol. 22, no. 3, pp. 328–351, 1998.

[36] R. R. Allan and G. E. Cook, "The long-period motion of the plane of a distant circular orbit," *Proceedings of the Royal Society A*, vol. 280, pp. 97–109, 1964.

[37] H. Lass and C. B. Solloway, "Motion of a satellite of the moon," *ARS Journal*, vol. 31, no. 2, pp. 220–222, 1961.

[38] E. Buchar, "Variational orbits of lunar satellites and their stability," in *Space Research Conference*, p. 999, 1963.

[39] P. d'Avanzo, P. Teofilatto, and C. Ulivieri, "Long-term effects on lunar orbiter," *Acta Astronautica*, vol. 40, no. 1, pp. 13–20, 1997.

[40] R. P. Russell and M. Lara, "Long-lifetime lunar repeat ground track orbits," *Journal of Guidance, Control, and Dynamics*, vol. 30, no. 4, pp. 982–993, 2007.

[41] S. L. Coffey, A. Deprit, and E. Deprit, "Frozen orbits for satellites close to an Earth-like planet," *Celestial Mechanics and Dynamical Astronomy*, vol. 59, pp. 37–72, 1994.

[42] G. E. Cook, "Perturbations of near-circular orbits by the Earth's gravitational potential," *Planetary and Space Science*, vol. 14, pp. 433–444, 1966.

[43] P. Gurfil and M. Lara, "Motion near frozen orbits as a means for mitigating satellite relative drift," *Celestial Mechanics and Dynamical Astronomy*, vol. 116, pp. 213–227, 2013.

[44] D. Scheeres, M. Guman, and B. Villac, "Stability analysis of planetary satellite orbiters: application to the europa orbiter," *Journal of Guidance, Control, and Dynamics*, vol. 24, no. 4, pp. 778–787, 2001.

[45] M. E. Paskowitz and D. J. Scheeres, "Design of science orbits about planetary satellites: application to europa," *Journal of Guidance, Control, and Dynamics*, vol. 29, no. 5, pp. 1147–1158, 2006.

[46] R. Broucke, "Numerical integration of periodic orbits in the main problem of artificial satellite theory," *Celestial Mechanics and Dynamical Astronomy*, vol. 58, pp. 99–123, 1994.

[47] A. Elipe and M. Lara, "Frozen orbits about the Moon," *Journal of Guidance, Control, and Dynamics*, vol. 26, pp. 238–243, 2003.

[48] D. Folta and D. Quinn, "Lunar frozen orbits," in *AIAA/AAS Astrodynamics Specialist Conference and Exhibit*, p. 6749, 2006.

[49] S. Tzirti, K. Tsiganis, and H. Varvoglis, "Quasi-critical orbits for artificial lunar satellites," *Celestial Mechanics and Dynamical Astronomy*, vol. 104, pp. 227–239, 2010.

[50] A. Abad, A. Elipe, and E. Tresaco, "Analytical model to find frozen orbits for a lunar orbiter," *Journal of Guidance, Control, and Dynamics*, vol. 32, pp. 888–898, 2009.

[51] S. Singh, R. Woollands, E. Taheri, and J. Junkins, "Feasibility of quasi-frozen, near-polar and extremely low-altitude lunar orbits," *Acta Astronautica*, vol. 166, pp. 450–468, 2020.

[52] E. Khattab, M. Radwan, and W. Rahoma, "Frozen orbits construction for a lunar solar sail," *Journal of Astronomy and Space Sciences*, vol. 37, pp. 1–9, 2020.

[53] S. Tzirti, K. Tsiganis, and H. Varvoglis, "Effect of 3rd-degree gravity harmonics and Earth perturbations on lunar artificial satellite orbits," *Celestial Mechanics and Dynamical Astronomy*, vol. 108, pp. 389–404, 2010.

[54] M. L. Lidov, "The evolution of orbits of artificial satellites of planets under the action of gravitational perturbations of external bodies," *Planetary and Space Science*, vol. 9, pp. 719–759, 1962.

[55] S. Tremaine, J. Touma, and F. Namouni, "Satellite dynamics on the Laplace surface," *The Astronomical Journal*, vol. 137, pp. 3706–3717, 2009.

[56] A. J. Rosengren, D. J. Scheeres, and J. W. McMahon, "The classical Laplace plane as a stable disposal orbit for geostationary satellites," *Advances in Space Research*, vol. 53, pp. 1219–1228, 2014.

[57] N. Sekiguchi, "On the libration of the orbital plane of a stationary artificial satellite with a circular orbit," *Publications of the Astronomical Society of Japan*, vol. 13, pp. 207–211, 1961.

[58] M. A. Vashkov'yak, "Stability of circular satellite orbits for combined action of perturbations from an external body and from the noncentrality of the planetary gravitational field," *Cosmic Research*, vol. 12, pp. 757–769, 1974.

[59] V. W. Kudielka, "Equilibria bifurcations of satellite orbits," in *The Dynamical Behaviour of our Planetary System* (R. Dvorak and J. Henrard, eds.), pp. 243–255, Dordrecht: Kluwer Academic Publishers, 1997.

[60] S. K. Singh, R. Woollands, E. Taheri, and J. Junkins, "Feasibility of quasi-frozen, near-polar and extremely low-altitude lunar orbits," *Acta Astronautica*, vol. 166, pp. 450–468, 2020.

[61] R. Allan and G. Cook, "The long-period motion of the plane of a distant circular orbit," *Proceedings of the Royal Society of London. Series A. Mathematical and Physical Sciences*, vol. 280, no. 1380, pp. 97–109, 1964.

[62] J. Carvalho, R. de Moraes, and A. Prado, "Some orbital characteristics of lunar artificial satellites," *Celestial Mechanics and Dynamical Astronomy*, vol. 108, pp. 371–388, 2010.